CALIFORNIA INSTITUTE OF TECHNOLOGY

EARTHQUAKE ENGINEERING RESEARCH LABORATORY

STUDIES ON THE EFFECT OF DIFFERENTIAL MOTIONS OF TWO FOUNDATIONS UPON THE RESPONSE OF THE SUPERSTRUCTURE OF A BRIDGE

Ahmed Mansour Abdel-Ghaffar

EERL 77-02

A Report on Research Conducted Under Grants
from the National Science Foundation

Pasadena, California

January 1977

BIBLIOGRAPHIC DATA SHEET	1. Report No. EERL 77-02	2.	3. Recipient's Accession No.
4. Title and Subtitle: Studies on the Effect of Differential Motions of Two Foundations upon the Response of the Superstructure of a Bridge			5. Report Date: January 1977 6.
7. Author(s): Ahmed M. Abdel-Ghaffar			8. Performing Organization Rept. No. EERL 77-02
9. Performing Organization Name and Address: California Institute of Technology, 1201 E. California Blvd., Pasadena, CA 91125			10. Project/Task/Work Unit No. 11. Contract/Grant No. NSF ENV74-19135
12. Sponsoring Organization Name and Address: National Science Foundation, Washington, D.C. 20550			13. Type of Report & Period Covered 14.

15. Supplementary Notes

16. Abstracts: This report contains two studies that were made of the effects of differential motion of the foundations upon the response of the superstructure of a bridge. The first study deals with the dynamic response of a "long beam" model of a bridge to both steady-state and random excitations applied at the supports. The harmonic and random end-excitations were analyzed in the frequency and time domains, respectively. The second study develops a method to analyze the dynamic soil-bridge interaction of a simple two-dimensional bridge model erected on an elastic half-space, with the input motion in the form of incident plane SH-waves. The bridge model consists of an elastic shear girder supported by two rigid abutments and rigid foundations which have a circular cross section and which are welded to the half-space. Finally, the dynamic response of the bridge and the effect of the radiative damping in the half-space on the interaction of the bridge are also studied.

17. Key Words and Document Analysis. 17a. Descriptors
Dynamic Structural Analysis (Structural Dynamics)
Beams (Supports)
Bridges (Girders)
Vibration (Frequencies and Modes)
Random Vibration
Dynamic Response
Foundation
Wave Propagation
Soil-Structure Interaction

17b. Identifiers/Open-Ended Terms

17c. COSATI Field/Group 1302 Civil Engineering 1313 Structural Engineering

18. Availability Statement	19. Security Class (This Report)	21. No. of Pages
Release unlimited.	UNCLASSIFIED	96
	20. Security Class (This Page) UNCLASSIFIED	22. Price PCA05 MFA01

ACKNOWLEDGMENTS

This report presents the results of research carried out at the California Institute of Technology during the years 1974-76 and originally appeared as part of the author's Ph. D. thesis (California Institute of Technology, May 1976). The author wishes to express gratitude to Professor G. W. Housner for his encouragement and constructive criticism. He is also grateful to Professor M. D. Trifunac and Dr. H. L. Wong, of the University of Southern California, for their collaboration on the soil-bridge interaction chapter. The interesting discussions with Professor T. K. Caughey are also greatly appreciated.

Much appreciation is expressed to the California Institute of Technology and the National Science Foundation for financial support during the course of this work. The partial support of this investigation by the U. S. Geological Survey is also acknowledged.

ABSTRACT

This report contains two studies that were made of the effects of differential motion of the foundations upon the response of the superstructure of a bridge. The first study deals with the dynamic response of a "long beam" model of a bridge to both steady-state and random excitations applied at the supports. The study has been simplified by considering a long shear beam, simply supported at two ends; this beam is subjected to two end excitations in the form of ground displacements. Harmonic excitations, differing in phase at the ends, were considered in the frequency domain by analyzing the steady state vibrations and calculating the displacement amplitudes at specific points on the beam. The energy content of the system has been presented, and the correlation between the two end excitations has been considered. For the random excitations, the analysis has been made in the time domain; two different cases of random motions have been considered.

The second study develops a method to analyze the dynamic soil-bridge interaction of a simple two-dimensional bridge model erected on an elastic half-space, with the input motion in the form of incident plane SH-waves. The bridge model consists of an elastic shear girder supported by two rigid abutments and rigid foundations which have a circular cross section and which are welded to the half-space. Finally, the dynamic response of the bridge and the effect of the radiative damping in the half-space on the interaction of the bridge are also studied.

STUDIES ON THE EFFECT OF DIFFERENTIAL MOTIONS OF TWO FOUNDATIONS UPON THE RESPONSE OF THE SUPERSTRUCTURE OF A BRIDGE

General Introduction

The effect of differential motions of two (or more) foundations upon the dynamic response of the superstructure of a bridge is a little understood problem which is of considerable interest in earthquake engineering. Although dynamic loadings acting on a bridge structure may result from different sources, including wind or vehicular motions, to the structural engineer one of the most important types of dynamic input is that produced by an earthquake. The definition of an appropriate ground-motion history is the most difficult and uncertain phase of the problem of predicting structural response to earthquakes. A common assumption in the usual treatment of earthquake excitations is that the same motion acts simultaneously at all points of the structure's foundation. If rotation motions are neglected, this assumption is equivalent to considering the foundation soil to be rigid. Such a hypothesis is not consistent with the concept of earthquake wave propagation; however, if the base dimensions of the structure are small relative to the vibration wave length in the soil, the assumption is acceptable. For example, if the velocity of the wave propagation is 6,000 ft/sec., a sinusoidal

wave of 3 Hz frequency will have a length of 2,000 ft., and a building with a base dimension of 100 ft. will be subjected to essentially the same motions over its entire length. On the other hand, a suspension bridge, which might have a length of several thousand feet, obviously would be subjected to drastically different motions at its two foundations. No direct measurements have been made on a bridge (or similar structure) at two widely separated foundations during an earthquake; however, it is evident that the motions must vary and their variance could contribute significantly to the dynamic response. Therefore, it is important to develop analytical procedures capable of dealing with multiple support excitation.

In order to lay a foundation from which later work, analyzing the dynamic response of long-span suspension bridges to earthquake ground motions applied at separate points of support, can be developed, two related topics have been studied in this report. The first topic, in Chapter I, deals with the dynamic response of a "long beam" model of a bridge span to both steady-state and random excitations applied at the supports; the results involve a large number of modes. The second topic, presented in Chapter II, develops a method to analyze the dynamic soil-bridge interaction of a simple bridge model erected on an elastic half-space, and the input motion is in the form of incident plane SH-waves. The dynamic response of the girder and the effect of the radiative damping in the half-space on the interaction of the girder are also studied.

CHAPTER I

DYNAMIC RESPONSE OF A LONG BEAM MODEL OF A BRIDGE STRUCTURE SUBJECT TO TWO END EXCITATIONS

I -1. Introduction

For long span structures such as suspension bridges, the piers or the abutments of the bridge may be far apart. In such a case, one may have a situation involving ground motion with different characteristics at each point of the bridge structure. For instance, during the 1971 San Fernando earthquake, the motions recorded by instruments located in Millikan library, at one end of the campus of California Institute of Technology, differed greatly from those of the Caltech Athenaeum located at the other end.

The following study deals with the effect of differential motions of two end supports upon the response of the superstructure. The study has been simplified by considering a long shear beam, simply supported at two ends, as shown in Fig. I-1, this beam is subjected to two end excitation, $f_1(t)$ and $f_2(t)$, in the form of ground displacements.

Two cases of excitation have been examined:

1. Harmonic excitations where

$$f_1(t) = A \sin \omega t \quad \text{and} \quad f_2(t) = A \sin (\omega t + \alpha)$$

in which A is the amplitude of the input motion and α is the phase difference between the two end excitations, as shown in Fig. I-1-a.

2. Random excitations where

$$f_1(t) = f_2(t) = f(t)$$

in which f(t) is a random function of time.

For the harmonic excitations, which may differ in phase at the ends, the analysis has been made in the frequency domain by considering the steady state vibrations and calculating the displacement amplitudes at certain points on the beam. The energy content of the system has been presented, and the correlation between the two end excitations has been considered.

For random excitations where $f_1(t) = f_2(t) = f(t)$, i.e., where the two ends of the shear beam have the same motion (symmetric mode shapes), the analysis has been made in the time domain; two cases of random motion have been considered: (1) Random motion (or displacement) of the supported ends that might be appropriate for a motion resulting from earthquake acceleration. This random motion was suggested by Shinozuka [1], and is in the form of the integral of a product of an envelope decaying deterministic function times a random function. (2) Random acceleration of the supported ends, which was developed by Tajima [8] from the work of Kanai [9], has been studied. The case where the excitation has a certain duration followed by free vibration has been considered.

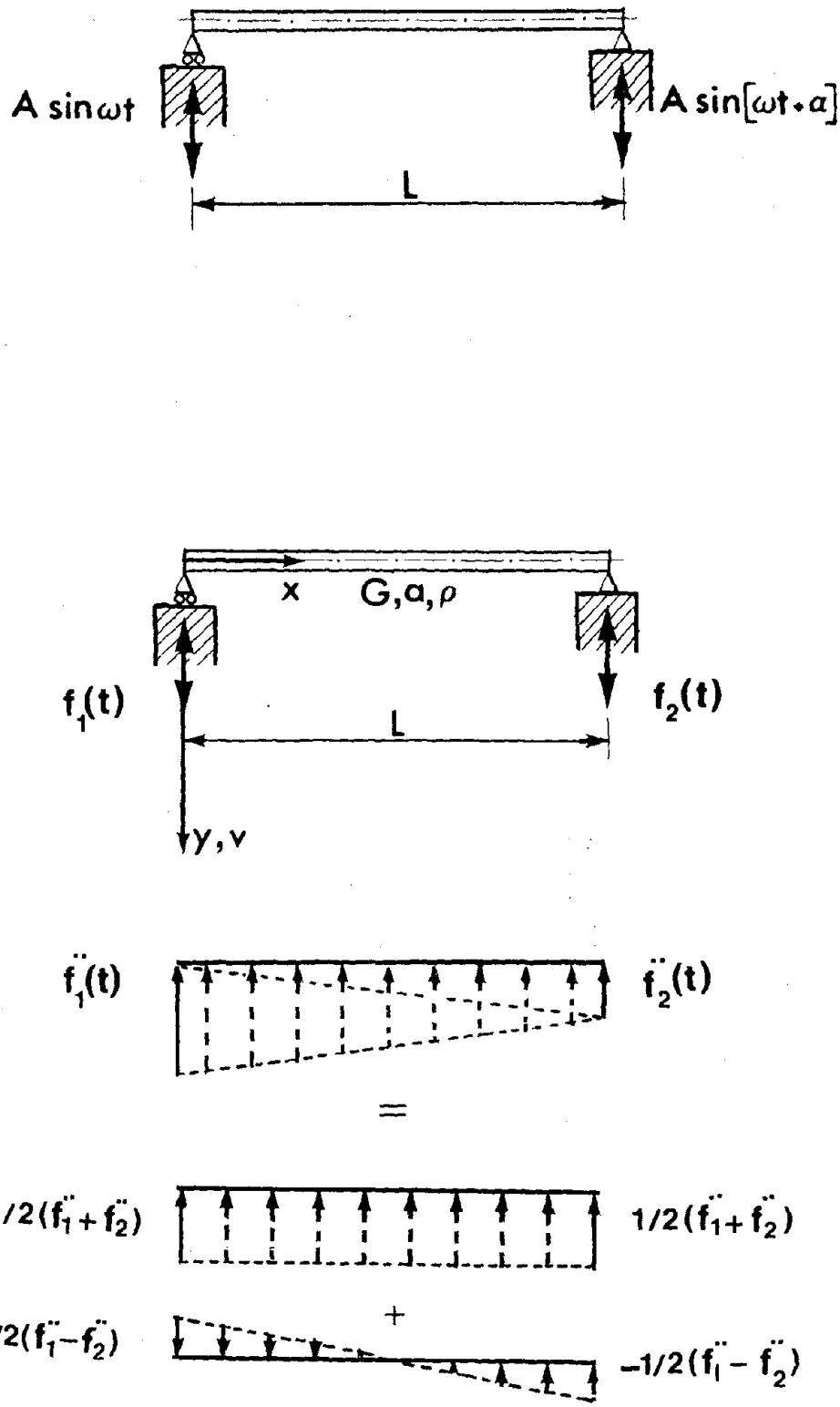

Fig. I-1. Bridge model subjected to motions at the support points.

In either case of random motion, the response of the beam structure has been calculated and plotted versus different cases of envelope functions for case (1) and different durations for case (2).

I-2. Steady-State Vibration Analysis

In this section, a study is made of the shear beam excited by the motion of the two support points, as shown in Fig. I-1-a. The two harmonic excitations, evidenced in the form of displacements, are of the same frequency and amplitude, but differ in phase by α. The steady-state vibration of the beam is studied, and the results are expressed in a nondimensional form that enables a concise graphical presentation of the dynamic characteristics of the system.

I-2-1. Undamped natural frequencies and mode shapes

The free vibration of the undamped shear beam is described by the equation of motion

$$\rho a \frac{\partial^2 v}{\partial t^2} = k' a G \frac{\partial^2 v}{\partial x^2} \quad , \tag{1.1}$$

where ρ is the mass density, a is the cross-sectional area of the beam, k' is a numerical factor depending on the shape of the cross-section, and G is the shear modulus. From Eq. 1.1, the eigenfunctions or mode shapes for the simply supported beam are

$$\Phi_n(x) = \sin \frac{n\pi x}{L} \quad , \qquad n = 1, 2, 3, 4, \ldots , \tag{1.2}$$

where L is the span length of the beam.

The natural frequencies are

$$\omega_n = \frac{n\pi}{L} \sqrt{\frac{k'G}{\rho}} \quad , \qquad n = 1, 2, 3, \ldots \quad . \tag{1.3}$$

Eqs. 1.2 and 1.3 are the n^{th} mode shape and the n^{th} natural frequency, with the understanding that these mode shapes and frequencies could be for fixed-end bridges as well as for hinged-end ones so long as they do not violate the boundary conditions of the displacement for such shear beams.

I-2-2. Equation of motion of damped shear beam

The differential equation of motion, in which a strain-rate type damping (relative damping) is assumed, can be written as

$$\rho \frac{\partial^2 v}{\partial t^2} = k' G \frac{\partial^2 v}{\partial x^2} + c \frac{\partial^3 v}{\partial t \, \partial x^2} \quad , \tag{1.4}$$

where c is the damping coefficient.

The initial and boundary conditions are

$$v(x, 0) = \dot{v}(x, 0) = 0 \quad , \tag{1.5}$$

$$\left.\begin{aligned} v(0, t) &= A \sin \omega t \quad , \\ v(L, t) &= A \sin (\omega t + \alpha) \quad , \end{aligned}\right\} \tag{1.6-a, 1.6-b}$$

where A is the amplitude of the two harmonic excitations, α is the phase difference, and ω is the frequency of the excitations.

I-2-3. Steady-state solution

For the steady-state vibration, the solution of Eq. 1.4 maybe written as

$$v(x, t) = X_1(x) \cos \omega t + X_2(x) \sin \omega t \quad , \tag{1.7}$$

where both $X_1(x)$ and $X_2(x)$ are functions of the spatial coordinate

x, only.

Substitution of Eq. 1.7 into Eq. 1.4 yields two simultaneous ordinary differential equations; putting these two equations in a matrix form containing the solutions and their derivatives, and then solving these four equations, one can obtain

$$X_1(x) = c_1 \cosh qx \cos px + c_2 \sinh qx \cos px + c_3 \sinh qx \sin px + c_4 \cosh qx \sin px \quad , \tag{1.8}$$

and

$$X_2(x) = -c_1 \sinh qx \sin px - c_2 \cosh qx \sin px + c_3 \cosh qx \cos px + c_4 \sinh qx \cos px \quad , \tag{1.9}$$

where c_1, c_2, c_3 and c_4 are arbitrary constants which can be determined from the boundary conditions (Eq. 1.6), and q, p and β are given by

$$q = \omega \sqrt{\frac{\rho}{k'G}} \sqrt{\left[\frac{\beta-1}{2\beta^2}\right]} \quad , \tag{1.10}$$

$$p = \omega \sqrt{\frac{\rho}{k'G}} \sqrt{\left[\frac{\beta+1}{2\beta^2}\right]} \quad , \tag{1.11}$$

$$\beta = \sqrt{1 + \left(\frac{c\omega}{k'G}\right)^2} \quad . \tag{1.12}$$

Upon using the boundary conditions (Eq. 1.6), the constants c_1, c_2, c_3, and c_4 are found to be

$$c_1 = 0 \quad , \tag{1.13}$$

$$c_2 = A\left[\frac{\sin\alpha \sinh qL \cos pL - \cos\alpha \cosh qL \sin pL + \cos pL \sin pL}{\sinh^2 qL \cos^2 pL + \cosh^2 qL \sin^2 pL}\right] \quad , \tag{1.14}$$

$$c_3 = A \quad , \tag{1.15}$$

$$c_4 = A\left[\frac{\sin\alpha \cosh qL \sin pL + \cos\alpha \sinh qL \cos pL - \sinh qL \cosh qL}{\cosh^2 qL \sin^2 pL + \sinh^2 qL \cos^2 pL}\right], \tag{1.16}$$

Therefore, at any point $\overset{*}{x}$ on the beam, the displacement can be written as

$$v(\overset{*}{x}, t) = X_1(\overset{*}{x}) \cos\omega t + X_2(\overset{*}{x}) \sin\omega t \quad , \tag{1.17-a}$$

or more conveniently as

$$v(\overset{*}{x}, t) = V_0(\overset{*}{x}) \sin(\omega t + \varphi) \quad , \tag{1.17-b}$$

where $V_0(\overset{*}{x})$ is the amplitude of the beam displacement at point $\overset{*}{x}$; it is expressed as

$$V_0(\overset{*}{x}) = \sqrt{X_1^2(\overset{*}{x}) + X_2^2(\overset{*}{x})} \quad . \tag{1.18}$$

In Eq. 1.17-b, φ is the phase angle between the displacement at that particular point $\overset{*}{x}$ and the harmonic motion of the left support (where $x = 0$ and $\alpha = 0$); φ is given by

$$\varphi(\overset{*}{x}) = \tan^{-1}\left[\frac{X_1(\overset{*}{x})}{X_2(\overset{*}{x})}\right] \quad . \tag{1.19}$$

To simplify the calculations, all the parameters involved in the steady-state solution are expressed in nondimensional form; for instance, define the dimensionless frequency $\overset{*}{\omega}$ as

$$\overset{*}{\omega} = \frac{\omega}{\omega_1} \quad , \tag{1.20}$$

where ω_1 is the fundamental natural frequency of the beam which is given by

$$\omega_1 = \frac{\pi}{L} \sqrt{\frac{k'G}{\rho}} \quad . \tag{1.21}$$

Therefore, Eqs. 1.10 and 1.11 become

$$q = \frac{\pi}{L} \overset{*}{\omega} \sqrt{\left[\frac{\beta-1}{2\beta^2}\right]} \quad , \tag{1.22}$$

and

$$p = \frac{\pi}{L} \overset{*}{\omega} \sqrt{\left[\frac{\beta+1}{2\beta^2}\right]} \quad . \tag{1.23}$$

Now, the steady-state solution, $v(x, t)$, can be expressed in terms of the normal modes $\Phi_n(x)$ as follows

$$v(x, t) = \sum_{n=1}^{\infty} \Phi_n(x)\, \eta_n(t) \tag{1.24}$$

where $\eta_n(t)$ is the n^{th} normal or generalized coordinate and is a function of time only.

Substitution of Eq. 1.24 into Eq. 1.4 yields

$$\ddot{\eta}_n(t) + \frac{c}{Gk'} \omega_n^2 \dot{\eta}_n(t) + \omega_n^2 \eta_n(t) = 0 \quad , \quad n = 1, 2, 3, \ldots \tag{1.25}$$

Let

$$\frac{c}{Gk'}\omega_n^2 = 2\omega_n\xi_n \quad , \tag{1.26}$$

where ξ_n is the damping ratio which is given by

$$\xi_n = \frac{1}{2}\omega_n\frac{c}{Gk'} \quad ; \tag{1.27}$$

then, one can obtain

$$\frac{c\omega}{Gk'} = 2\xi_n\frac{\omega}{\omega_n} = 2\xi_1\frac{\omega}{\omega_1} = 2\xi_1\overset{*}{\omega} \tag{1.28}$$

where ξ_1 is the damping ratio of the first mode. Therefore, Eq. 1.12 becomes

$$\beta = \sqrt{1+(2\xi_1\overset{*}{\omega})^2} \quad . \tag{1.29}$$

I-2-4. Dynamic response of the beam (numerical results)

With the aid of Eqs. 1.17, 1.18 and 1.19, the displacement $v(x, t)$, and the phase angle $\varphi(x)$ were computed at three different points of the beam: at $x = \frac{L}{2}$, $\frac{L}{4}$ and $\frac{3L}{4}$. The damping for the first mode was assumed to be 2%, and α was given several values: 0°, 45°, 90°, 135° and 180°. Figures I-2, I-4 and I-6 show the displacement amplitudes $V_0\left(\frac{L}{2}\right)$, $V_0\left(\frac{L}{4}\right)$ and $V_0\left(\frac{3L}{4}\right)$ as functions of the dimensionless frequency $\overset{*}{\omega}$, with the excitation phase angle α as a parameter. From these figures the following observations may be made.

1. In all cases, the amplitude curves for different values of the phase angle α, all have the same value $\left(|V_0| = 1.0\right)$ when $\overset{*}{\omega}$ approaches 0.
2. At the mid-point of the span $\left(\left|V_0\left(\frac{L}{2}\right)\right|, \text{ Fig. I-2}\right)$, there is no contribution from the even modes (antisymmetric mode shapes), because that point $\left(\overset{*}{x} = \frac{L}{2}\right)$ is always a node point for these mode shapes.
3. In Fig. I-2, also, the maximum displacement is attained when $\alpha = 0^\circ$, i.e., when the two harmonic end-excitations are in phase, and this maximum (or peak value) decreases as α increases in all the odd modes (symmetric mode shapes). Further understanding of this behavior of the system may be obtained by studying Fig. I-3 which corresponds to Fig. I-2. In Fig. I-3, when $\alpha = 0^\circ$ to $\alpha \simeq 60^\circ$ the rate of decrease is very slow, while from $\alpha \simeq 60^\circ$ to $\alpha = 180^\circ$, the rate of decrease is very rapid.
4. Because of the type of damping assumed, the contribution from the third mode, in Figs. I-2 and I-3, is smaller than the contribution from the first mode (by about 80%).
5. At the points $\left|V_0\left(\frac{L}{4}\right)\right|$ and $\left|V_0\left(\frac{3L}{4}\right)\right|$, the results are almost identical, as seen from Figs. I-4, I-5, I-6 and I-7. There is no contribution from the fourth mode where there are nodes at these points $\left(\overset{*}{x} = \frac{L}{4} \text{ and } \frac{3L}{4}\right)$. For different values of the angle α, the behavior of the system at the second mode is completely different from the behavior at the first mode.

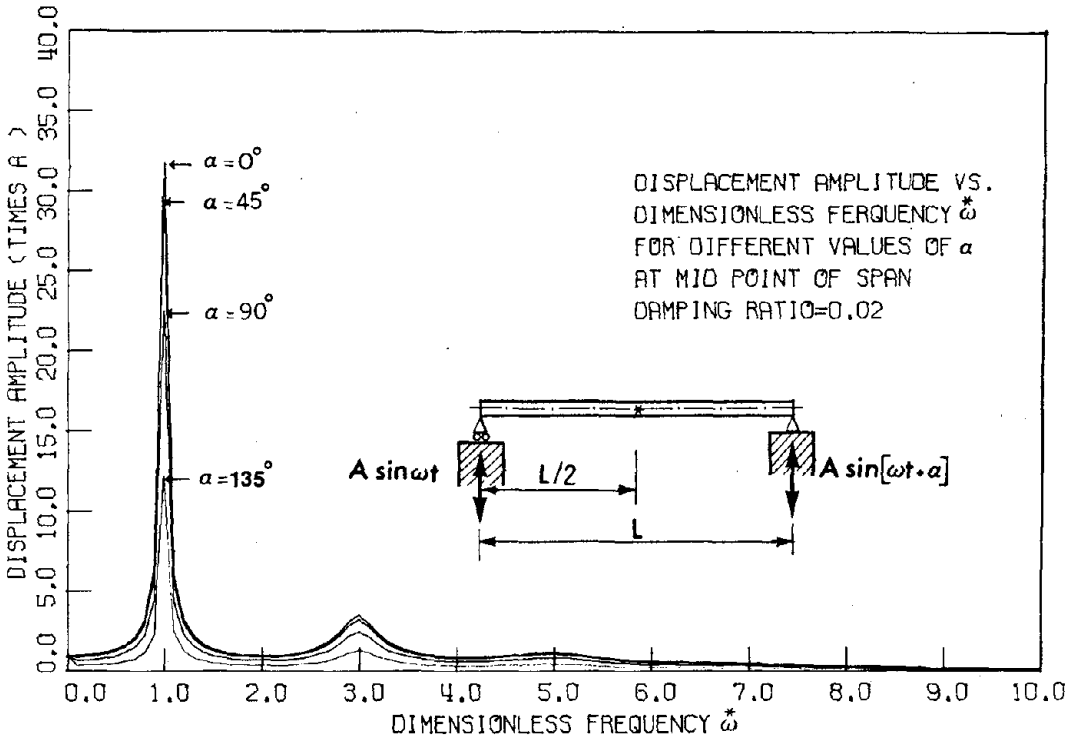
DISPLACEMENT AMPLITUDE (TIMES A)
0.0
5.0
10.0
15.0
20.0
25.0
30.0
35.0
40.0
α = 0°
α = 45°
α = 90°
α = 135°
DISPLACEMENT AMPLITUDE VS.
DIMENSIONLESS FERQUENCY ω*
FOR DIFFERENT VALUES OF α
AT MID POINT OF SPAN
DAMPING RATIO=0.02
A sinωt
L/2
L
A sin[ωt+α]
0.0
1.0
2.0
3.0
4.0
5.0
6.0
7.0
8.0
9.0
10.0
DIMENSIONLESS FREQUENCY ω*

Fig. I-2

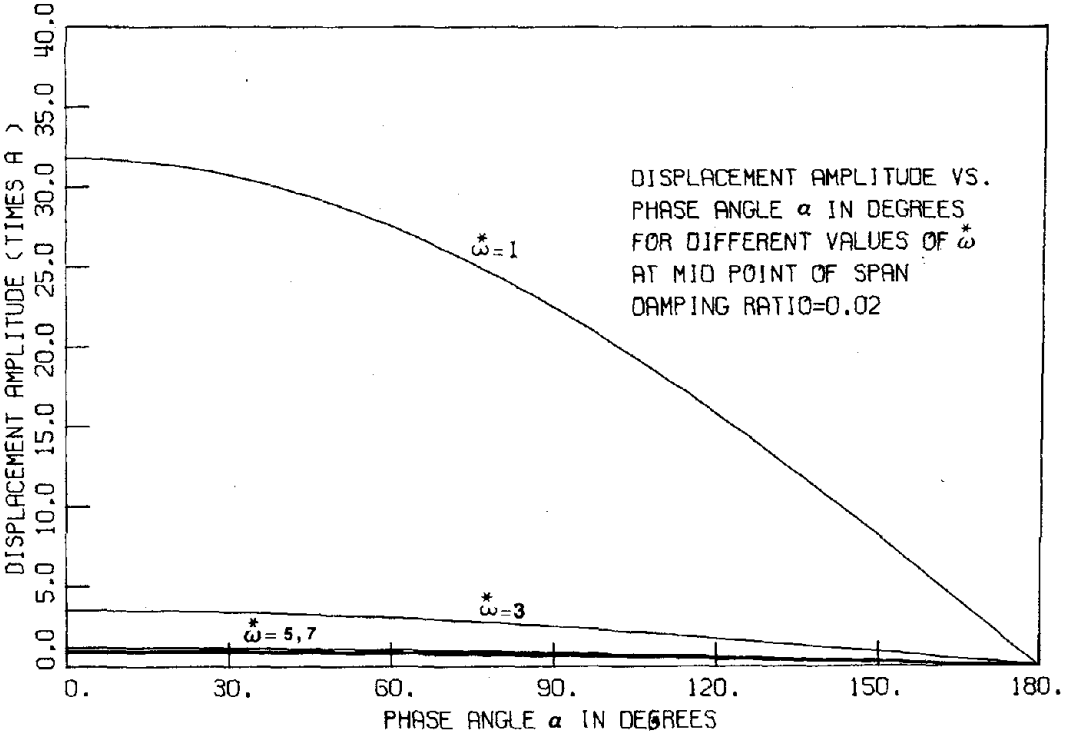
DISPLACEMENT AMPLITUDE (TIMES A)
0.0
5.0
10.0
15.0
20.0
25.0
30.0
35.0
40.0
DISPLACEMENT AMPLITUDE VS.
PHASE ANGLE α IN DEGREES
FOR DIFFERENT VALUES OF ω*
AT MID POINT OF SPAN
DAMPING RATIO=0.02
ω*=1
ω*=3
ω*=5,7
0.
30.
60.
90.
120.
150.
180.
PHASE ANGLE α IN DEGREES

Fig. I-3

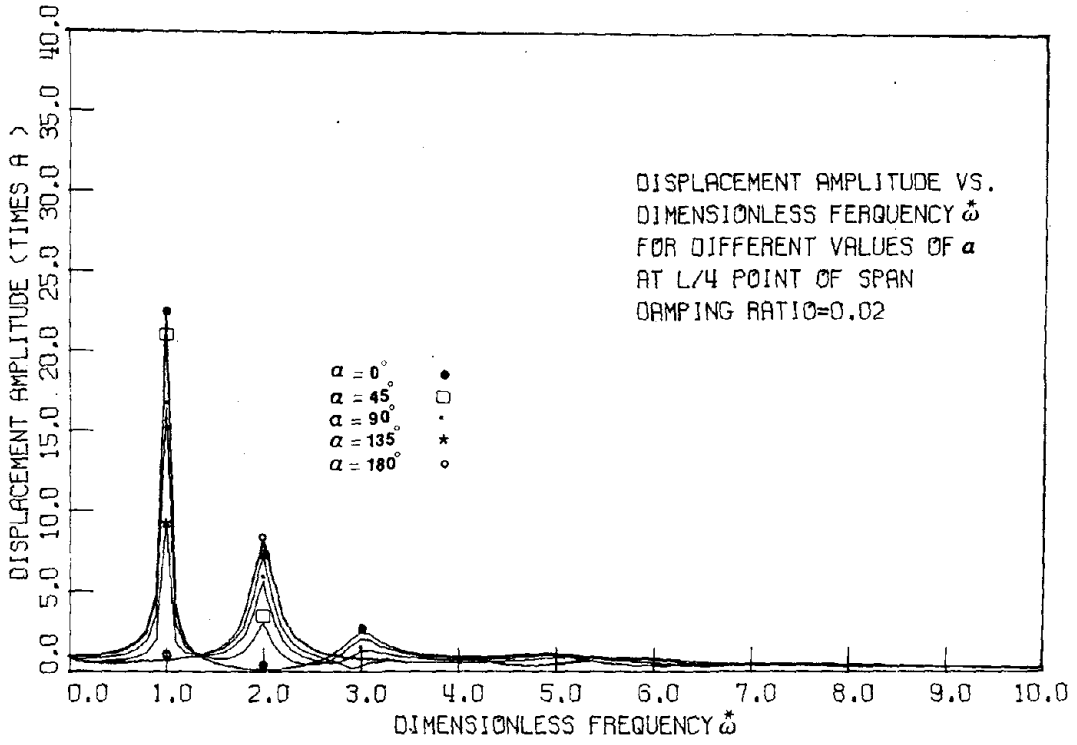
DISPLACEMENT AMPLITUDE VS.
DIMENSIONLESS FERQUENCY $\bar{\omega}$
FOR DIFFERENT VALUES OF α
AT L/4 POINT OF SPAN
DAMPING RATIO=0.02
$\alpha = 0^\circ$
$\alpha = 45^\circ$
$\alpha = 90^\circ$
$\alpha = 135^\circ$
$\alpha = 180^\circ$
DISPLACEMENT AMPLITUDE (TIMES A)
0.0 5.0 10.0 15.0 20.0 25.0 30.0 35.0 40.0
0.0 1.0 2.0 3.0 4.0 5.0 6.0 7.0 8.0 9.0 10.0
DIMENSIONLESS FREQUENCY $\bar{\omega}$

Fig. I-4

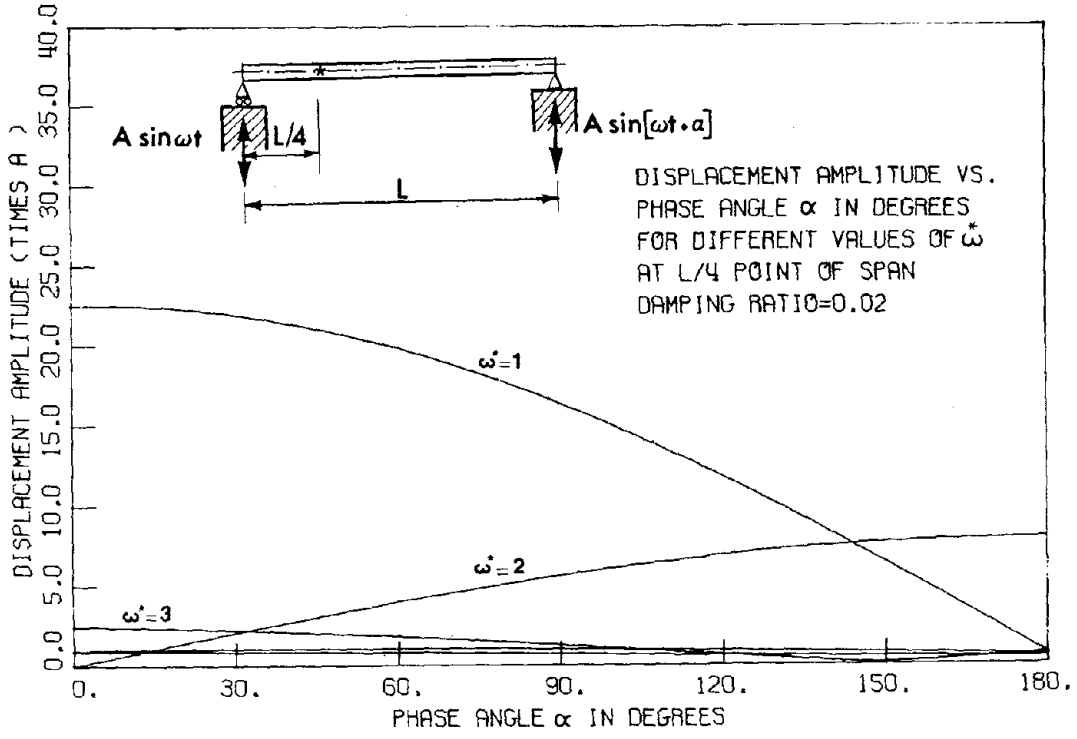
A sinωt
L/4
L
A sin[ωt+α]
DISPLACEMENT AMPLITUDE VS.
PHASE ANGLE α IN DEGREES
FOR DIFFERENT VALUES OF $\bar{\omega}$
AT L/4 POINT OF SPAN
DAMPING RATIO=0.02
$\bar{\omega}=1$
$\bar{\omega}=2$
$\bar{\omega}=3$
DISPLACEMENT AMPLITUDE (TIMES A)
0.0 5.0 10.0 15.0 20.0 25.0 30.0 35.0 40.0
0. 30. 60. 90. 120. 150. 180.
PHASE ANGLE α IN DEGREES

Fig. I-5

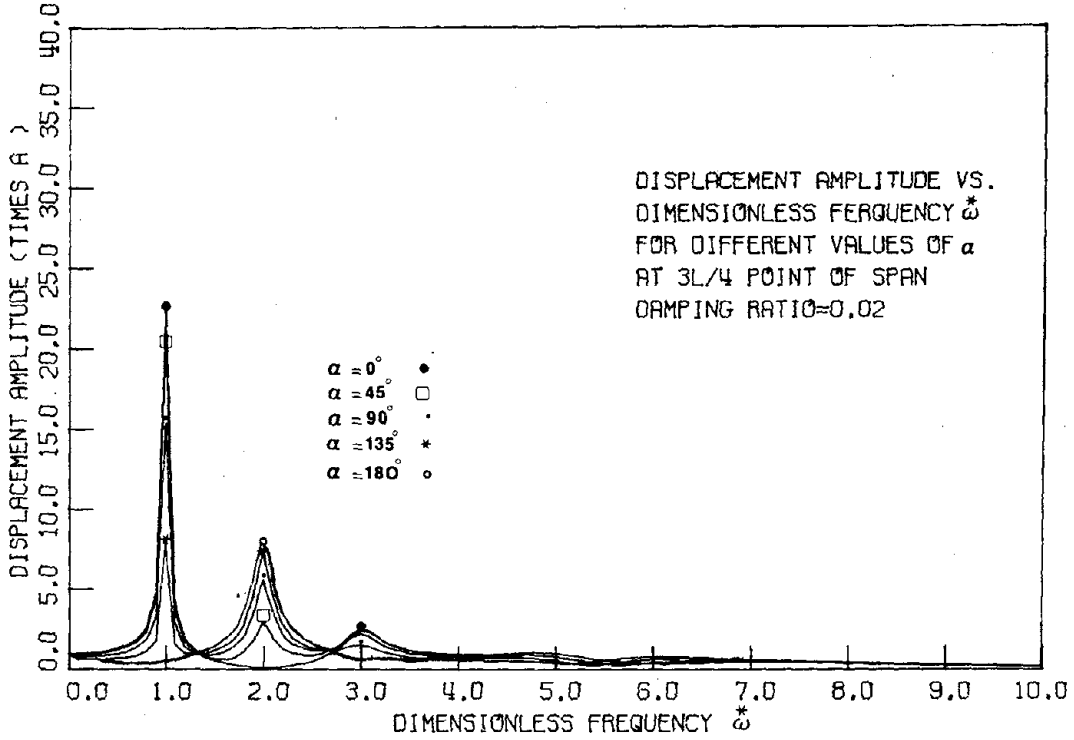
DISPLACEMENT AMPLITUDE (TIMES A)
0.0 5.0 10.0 15.0 20.0 25.0 30.0 35.0 40.0
DISPLACEMENT AMPLITUDE VS.
DIMENSIONLESS FERQUENCY ω^*
FOR DIFFERENT VALUES OF α
AT 3L/4 POINT OF SPAN
DAMPING RATIO=0.02
α =0°
α =45°
α =90°
α =135°
α =180°
0.0 1.0 2.0 3.0 4.0 5.0 6.0 7.0 8.0 9.0 10.0
DIMENSIONLESS FREQUENCY ω^*

Fig. I-6

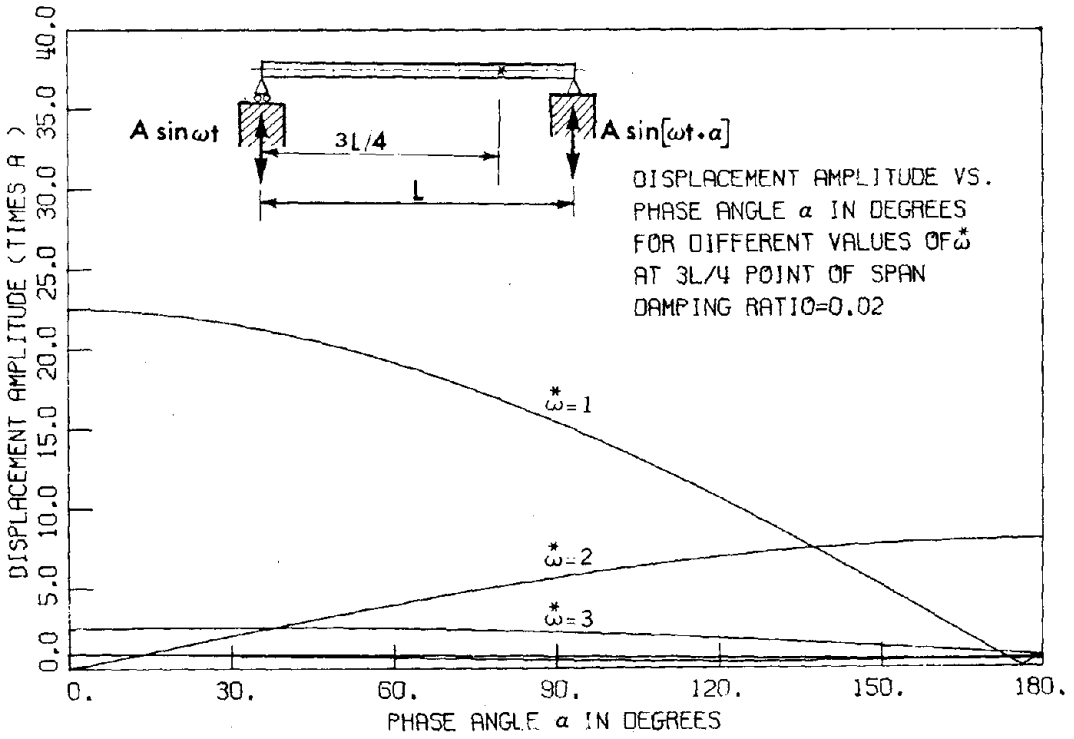
DISPLACEMENT AMPLITUDE (TIMES A)
0.0 5.0 10.0 15.0 20.0 25.0 30.0 35.0 40.0
A sinωt
3L/4
L
A sin[ωt+α]
DISPLACEMENT AMPLITUDE VS.
PHASE ANGLE α IN DEGREES
FOR DIFFERENT VALUES OF ω^*
AT 3L/4 POINT OF SPAN
DAMPING RATIO=0.02
ω^*=1
ω^*=2
ω^*=3
0. 30. 60. 90. 120. 150. 180.
PHASE ANGLE α IN DEGREES

Fig. I-7

6. The phase difference φ between the response and the left-support excitation (Eqs. 1.17-b and 1.19), has been plotted for these three points on the beam, as a function of the dimensionless frequency $\overset{*}{\omega}$, and with α as a parameter. All three sets of curves in Figs. I-8, I-9 and I-10 indicated that during resonance of the first mode, the external forced displacement at the left support and the response have a phase difference of $\frac{\pi}{2}$.
7. By comparing Figs. I-9 and I-10, a considerable difference is seen in the phase characteristics of the two cases when $\overset{*}{x} = \frac{L}{4}$ and $\frac{3L}{4}$, in contrast with the similarity of the amplitude characteristics (in the frequency domain) shown in Figs. I-4, I-5, I-6 and I-7.

I-2-5. Energy consideration

For an external force $F(x, t)$, the equation of motion (Eq. 1.4) can be written as

$$\rho \frac{\partial^2 v}{\partial t^2} = Gk' \frac{\partial^2 v}{\partial x^2} + c \frac{\partial^2 v}{\partial t \partial x^2} + F(x, t) \qquad (1.30)$$

In terms of the inertia forces which result from the two end motions, $F(x, t)$ can be described, as shown in Fig. I-1-c, as

$$F(x, t) = \rho \left[\left(1 - \frac{x}{L}\right) \ddot{f}_1(t) + \frac{x}{L} \ddot{f}_2(t) \right] . \qquad (I.31)$$

Because $f_1(t) = A \sin \omega t$ and $f_2(t) = A \sin(\omega t + \alpha)$, Eq. 1.31 becomes

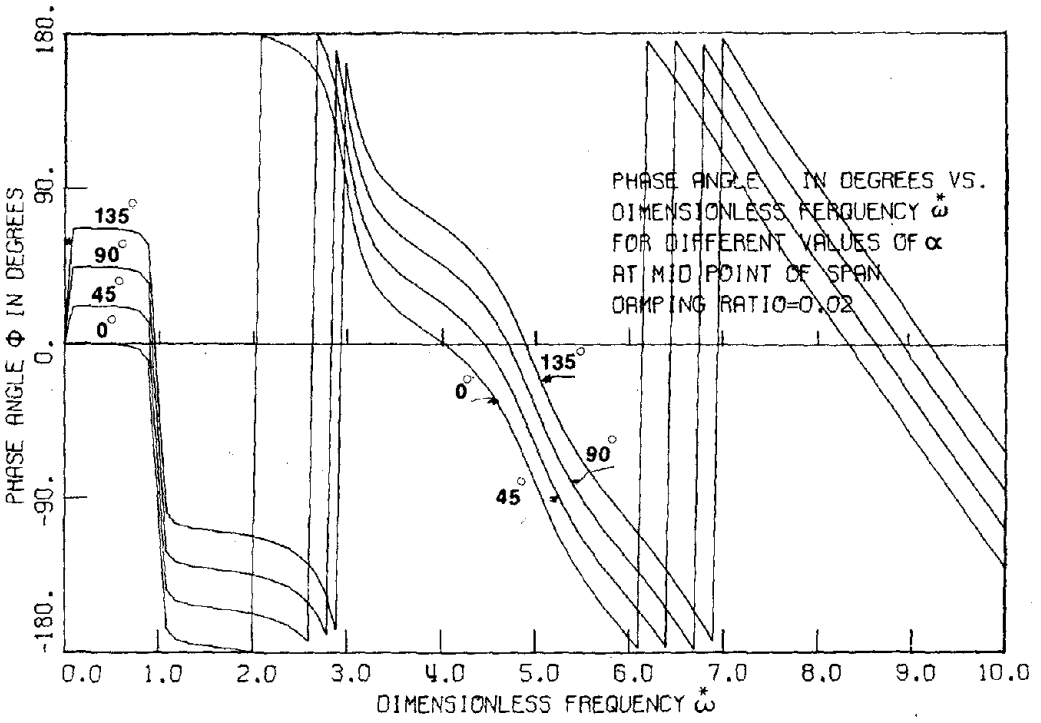
PHASE ANGLE Φ IN DEGREES VS.
DIMENSIONLESS FERQUENCY ω*
FOR DIFFERENT VALUES OF α
AT MID POINT OF SPAN
DAMPING RATIO=0.02
PHASE ANGLE Φ IN DEGREES
DIMENSIONLESS FREQUENCY ω*
180.
90.
0.
-90.
-180.
0.0
1.0
2.0
3.0
4.0
5.0
6.0
7.0
8.0
9.0
10.0
135°
90°
45°
0°

Fig. I-8

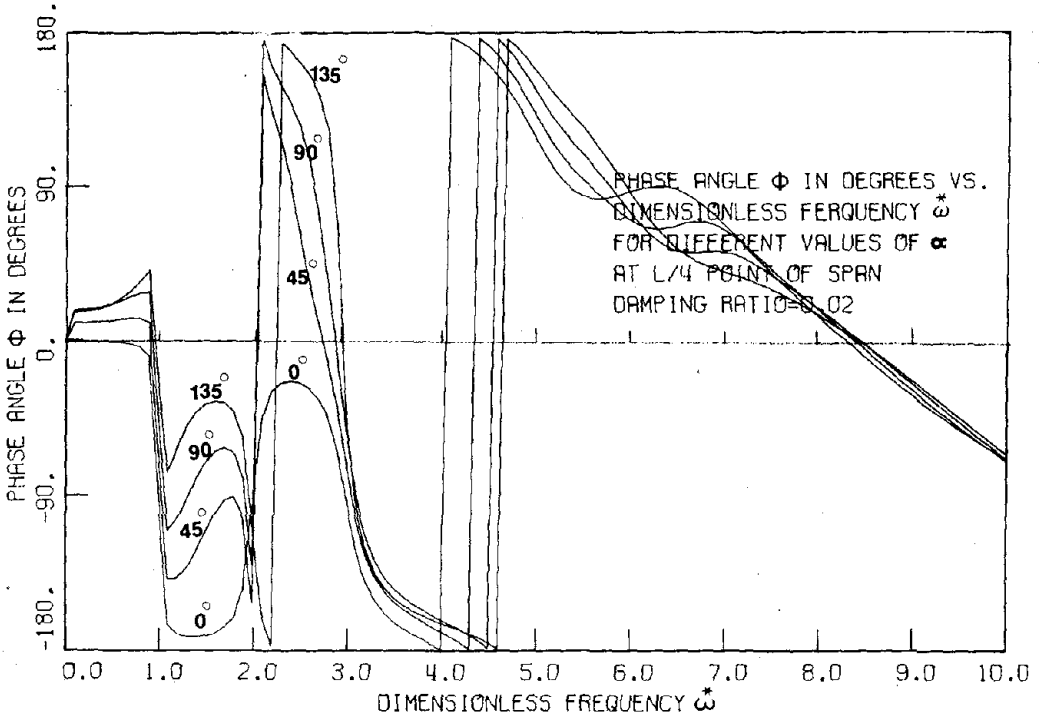
PHASE ANGLE Φ IN DEGREES VS.
DIMENSIONLESS FERQUENCY ω*
FOR DIFFERENT VALUES OF α
AT L/4 POINT OF SPAN
DAMPING RATIO=0.02
PHASE ANGLE Φ IN DEGREES
DIMENSIONLESS FREQUENCY ω*
180.
90.
0.
-90.
-180.
0.0
1.0
2.0
3.0
4.0
5.0
6.0
7.0
8.0
9.0
10.0
135°
90°
45°
0°

Fig. I-9

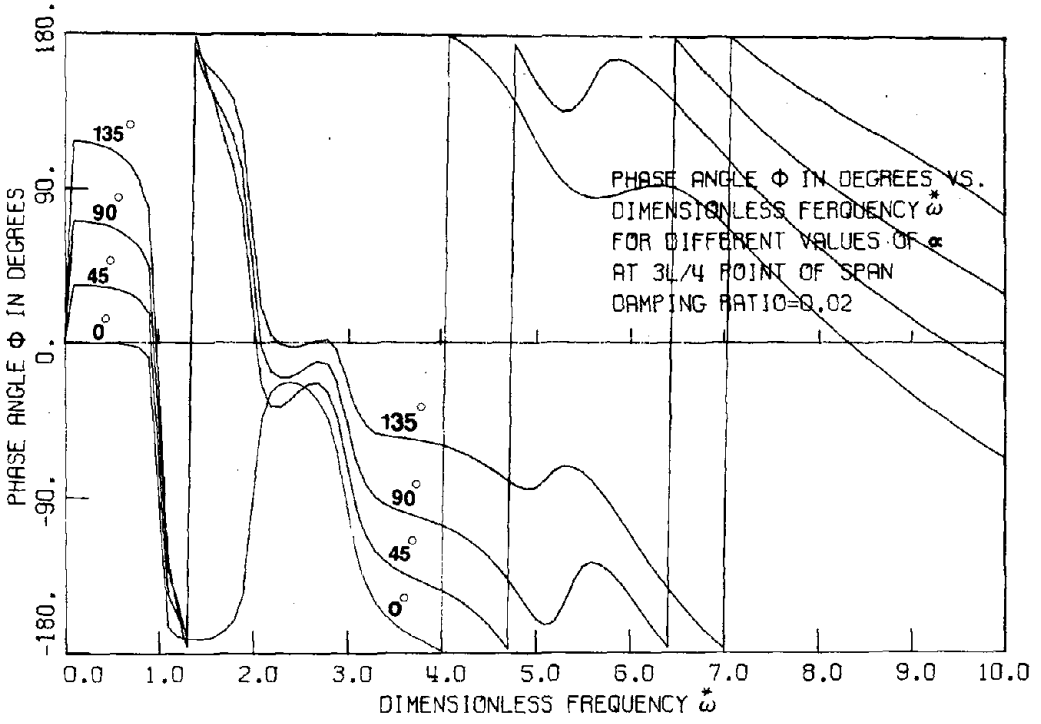

Fig. I-10

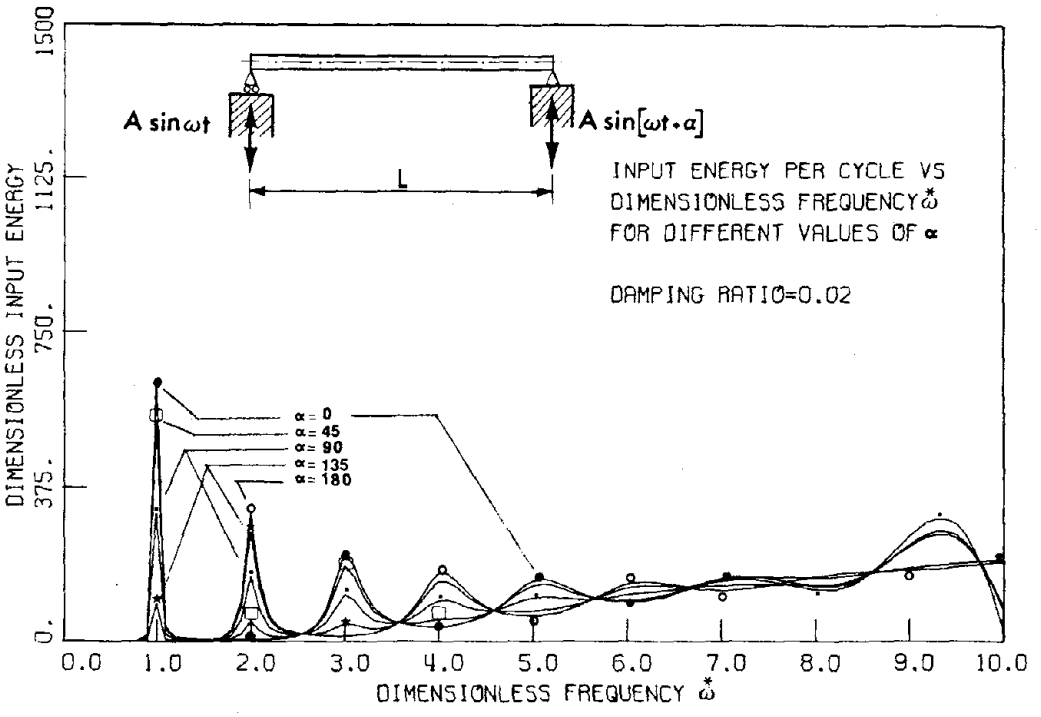

Fig. I-11

$$F(x,t) = \rho A\left[-\omega^2 \sin\omega t - \omega^2 \frac{x}{L}(\sin\omega t\cos\alpha + \cos\omega t \sin\alpha - \sin\omega t)\right] . \quad (1.32)$$

Therefore, the amount of energy input into the system, which is supplied by the harmonically excited motions is

$$E_I(t) = \int_0^L F(x,t)\frac{\partial v}{\partial t}\, dt\, dx \ , \quad (1.33)$$

and the energy per cycle of the vibration is

$$E_I/\text{cycle} = \int_0^L \int_0^{\frac{2\pi}{\omega}} F(x,t)\frac{\partial v}{\partial t}\, dt\, dx \ . \quad (1.34)$$

This energy was calculated and plotted in dimensionless form $\overset{*}{E}_I$, as

$$\overset{*}{E}_I = \left(\frac{E_I/\text{cycle}}{\frac{ak'G}{L} \cdot A^2}\right) \ . \quad (1.35)$$

Fig. I-11 shows $\overset{*}{E}_I$ versus $\overset{*}{\omega}$ with α as a parameter. At resonance, this energy input is equal to the energy dissipated by the system due to damping. Fig. I-11 shows the increase of this energy in the higher modes. The contribution from the odd symmetric modes and the even antisymmetric modes are shown to be proportional with the phase angle α . Finally, the energy of vibration as seen in Fig. I-11, is greatest in the normal modes of low order; this is to be expected because to excite the lower modes requires more energy.

A similar analysis was made for both the kinetic and strain energies of the system. The kinetic energy is

$$T(t) = \frac{1}{2} \int_0^L \rho a \left(\frac{\partial v}{\partial t}\right)^2 dx \quad , \tag{1.36}$$

and the mean value of this kinetic energy per cycle is

$$T_{mean}/cycle = \frac{1}{2} \frac{\omega}{2\pi} \int_0^L \int_0^{\frac{2\pi}{\omega}} \rho a \left(\frac{\partial v}{\partial t}\right)^2 dt\, dx \quad . \tag{1.37}$$

The strain energy of the system is

$$U(t) = \frac{1}{2} \int_0^L k' a G \left(\frac{\partial v}{\partial x}\right)^2 dx \quad , \tag{1.38}$$

and the mean value of this energy per cycle is

$$U_{mean}/cycle = \frac{1}{2} \frac{\omega}{2\pi} \int_0^L \int_0^{\frac{2\pi}{\omega}} k' a G \left(\frac{\partial v}{\partial x}\right)^2 dt\, dx \quad . \tag{1.39}$$

This strain energy is due to shear alone, because any element of the beam may undergo distortion but no rotation.

Expressing these energies in nondimensional form, one obtains

$$\overset{*}{T} = \left(\frac{T_{mean}/cycle}{\frac{k' a G}{L} \cdot A^2} \right) \quad , \tag{1.40}$$

and

$$\overset{*}{U} = \left(\frac{U_{mean}/cycle}{\frac{k' a G}{L} \cdot A^2} \right) \quad . \tag{1.41}$$

Figs. I-12 and I-13 show these two dimensionless energies as functions of $\overset{*}{\omega}$; they are almost equal at each normal mode.

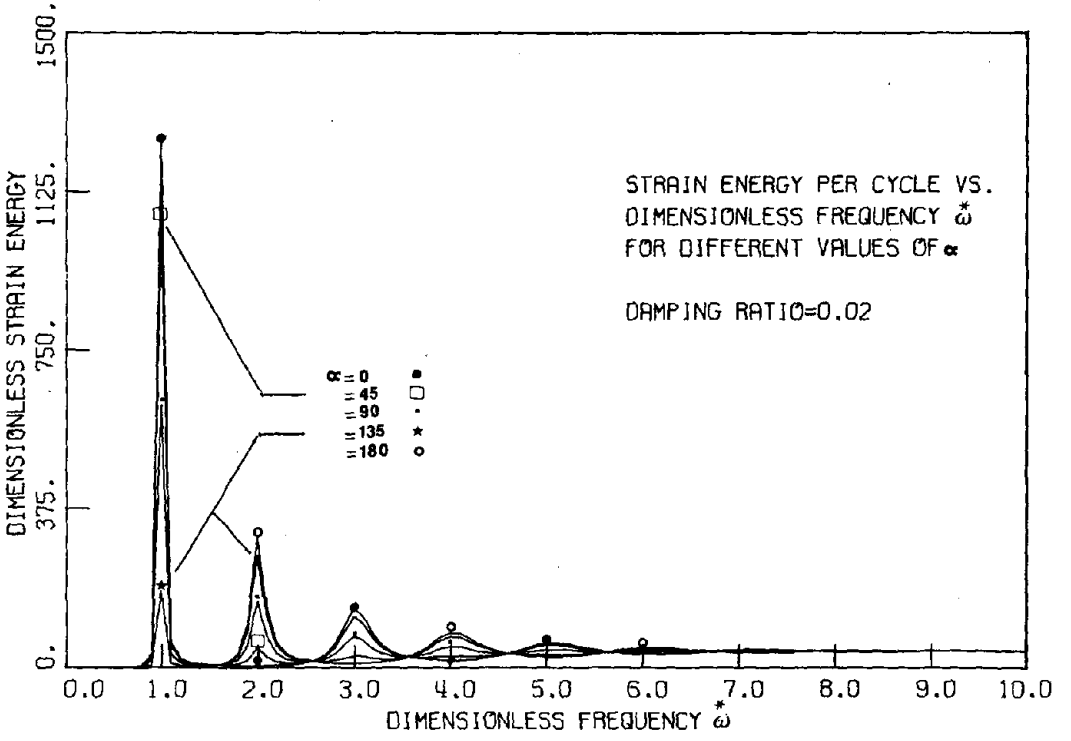

Fig. I-12

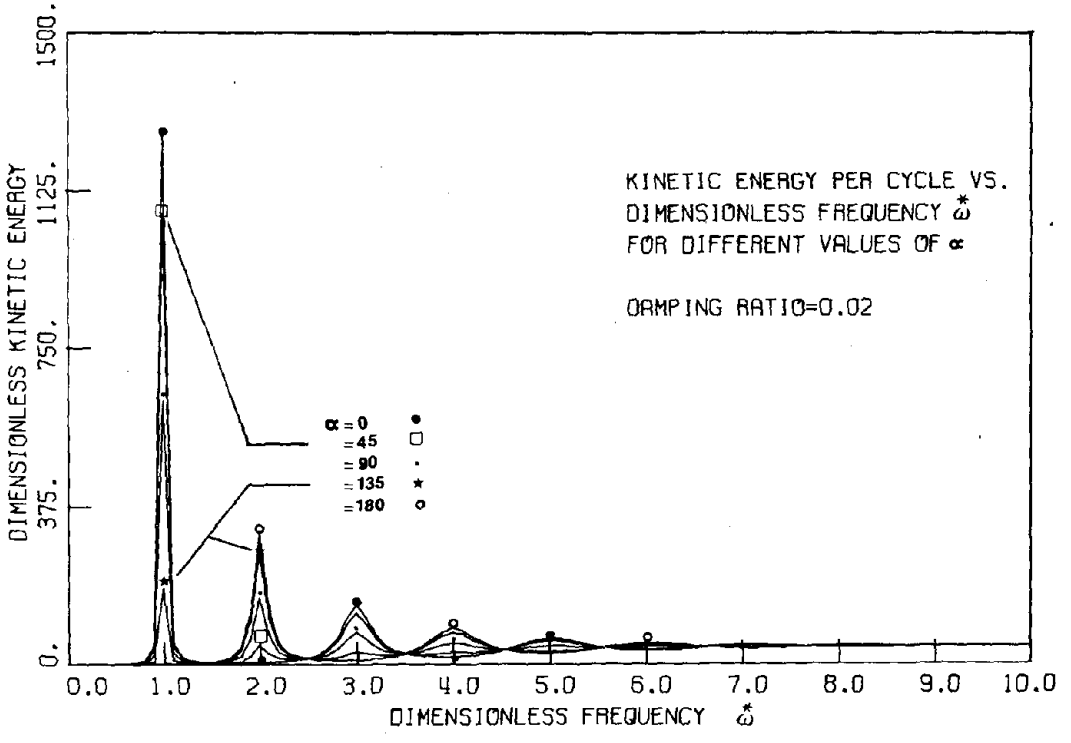

Fig. I-13

I-3. Random Vibration Analysis

This section contains a discussion of the transient response of the beam to random excitations applied at the support points. The analysis has been confined to the stationary aspects of the motion. Two types of input motion having various specific characteristics were considered, and the mean square displacement was calculated for both cases. The two end excitations were assumed to be identical in both cases.

I-3-1. Equation of motion

Substituting Eq. 1.24 into Eq. 1.30, with $F(x, t)$ defined as in Eq. 1.31, one can obtain the following, after multiplying both sides of the resulting equation by $\Phi_m(x)$, integrating from 0 to L with respect to x, and making use of the orthogonality of the modes.

$$\ddot{\eta}_n(t) + 2\omega_n \xi_n \dot{\eta}_n(t) + \omega_n^2 \eta_n(t) = \frac{2}{n\pi} [\ddot{f}_1(t) - (-1)^n \ddot{f}_2(t)] \quad , \quad n = 1, 2, 3, \ldots \tag{1.42}$$

By considering Fig. I-1-c, one can decompose the two triangular inertia forces to the symmetric case where one has $\frac{1}{2}\left(\ddot{f}_1(t) + \ddot{f}_2(t)\right)$, and the antisymmetric case where one has $\frac{1}{2}\left(\ddot{f}_1(t) - \ddot{f}_2(t)\right)$; using Eq. 1.42, these two cases can be written as

$$\ddot{\eta}_n(t) + 2\omega_n \xi_n \dot{\eta}_n(t) + \omega_n^2 \eta_n(t) = \frac{2}{n\pi} \left(\ddot{f}_1(t) + \ddot{f}_2(t)\right) \quad , \quad n = 1, 3, 5, \ldots \tag{1.43}$$

which includes the contributions from the odd modes (symmetric mode shapes), and

$$\ddot{\eta}_n(t) + 2\omega_n \xi_n \dot{\eta}_n(t) + \omega_n^2 \eta_n(t) = \frac{2}{n\pi} \left(\ddot{f}_1(t) - \ddot{f}_2(t) \right) \quad , \qquad n = 2, 4, 6, \ldots \tag{1.44}$$

which includes the contributions from the even modes (antisymmetric mode shapes).

Because this analysis considers that $f_1(t) = f_2(t) = f(t)$, where $f(t)$ is a random input motion, it shows only the contributions from the symmetric modes. Accordingly, Eqs. 1.43 and 1.44 reduce to

$$\ddot{\eta}_n(t) + 2\omega_n \xi_n \dot{\eta}_n(t) + \omega_n^2 \eta_n(t) = \frac{4}{n\pi} \ddot{f}(t) \quad , \qquad n = 1, 3, 5, \ldots \tag{1.45}$$

If the initial conditions are assumed to be zero, a valid solution of Eq. 1.45 is obtained through the time domain using the convolution, or Duhamel, integral

$$\eta_n(t) = \frac{4}{n\pi} \int_0^t h(t-\tau)\, \ddot{f}(\tau)\, d\tau \quad , \qquad n = 1, 3, 5, \ldots \tag{1.46}$$

in which τ is a dummy time variable and $h(t)$ is the unit-impulse-response function of the system; it is expressed by

$$\left.\begin{aligned} h(t) &= \frac{1}{\omega_{dn}} e^{-\xi_n \omega_n t} \sin \omega_{dn} t \quad , && t \geq 0 \\ &= 0 && t < 0 \end{aligned}\right\} \quad , \tag{1.47}$$

with $\omega_{dn} = \sqrt{1 - \xi_n^2}\ \omega_n$ as the damped natural frequency.

The stochastic mean square of the normal coordinate of Eq. 1.46 can be written as

$$\langle \eta_n^2(t) \rangle = \left(\frac{4}{n\pi}\right)^2 \int_0^t \int_0^t h(t-\tau)\, h(t-\tau')\, \langle \ddot{f}(\tau)\, \ddot{f}(\tau') \rangle \, d\tau \, d\tau' \quad , \quad n = 1, 3, 5, \ldots \tag{1.48}$$

where $\ddot{f}(t)$ is assumed to be mean square continuous. The quantity $\langle \ddot{f}(\tau)\ddot{f}(\tau') \rangle$ is, by definition, $R_{\ddot{f}}(\tau, \tau')$, which is the autocorrelation function for $\ddot{f}(\tau)$. The autocorrelation function for a stationary process depends only on the time difference $(\tau - \tau')$, and not on τ and τ' individually.

The random excitation has been considered as either

(1) Random imput displacement f(t) with specific characteristics, or

(2) Random input acceleration $\ddot{f}(t)$ with specific duration and other definite characteristics.

I-3-2. Dynamic response under random displacements

The particular form of random motion considered for the random function f(t) (case (1) above) might express ground motion resulting from earthquake acceleration as stated by Shinozuka and Henry [1]. Unfortunately, the amount of data on strong motion earthquakes is quite limited, so it has not been possible to obtain anything like a complete statistical description of earthquakes. However, there has been previous work concerning the statistical nature of ground motion; reference is made to studies by Bogdanoff, Goldberg and Bernard [3], Bolotin [4], Rosenblueth and Bustamante [5], Caughey and Stumpf [2], Sharpe, et al. [6], and Housner and Jennings [7].

The random displacement $f(t)$ suggested by Shinozuka and Henry [1] was based on the evident condition that the ground velocity $\dot{f}(t)$ must approach zero as time t approaches infinity. This ground displacement is in the form of the integral of the envelope deterministic time function times a random function having specific properties:

$$f(t) = \int_0^t G(\tau)\, g(\tau)\, d\tau \quad , \tag{1.49}$$

where $G(t)$ is the envelope function; it is expressed by

$$G(t) = (e^{-\alpha t} - e^{-\beta t}) \quad , \qquad \beta > \alpha > 0 \quad ; \tag{1.50}$$

α and β are constants.

The random function $g(t)$ has the following properties:

1. $g(t)$ is stationary
2. $g(t)$ is Gaussian
3. $g(t)$ has mean zero, i.e., $\langle g(t) \rangle = 0$
4. $g(t)$ has power spectrum $\Psi(\omega)$
5. $\dot{g}(t)$ exists and is continuous in mean square; moreover, because $g(t)$ is stationary and Gaussian, so is $\dot{g}(t)$.

Hence, $\dot{g}(t)$ and $\ddot{g}(t)$ are Gaussian and continuous in mean square with mean $\langle \dot{g}(t) \rangle = \langle \ddot{g}(t) \rangle = 0$.

From Eq. 1.49, the expressions for the velocity and the acceleration are

$$\dot{f}(t) = (e^{-\alpha t} - e^{-\beta t})\, g(t) \quad , \tag{1.51}$$

and

$$\ddot{f}(t) = (-\alpha e^{-\alpha t} + \beta e^{-\beta t})\, g(t) + (e^{-\alpha t} - e^{-\beta t})\, \dot{g}(t) \quad . \qquad (1.52)$$

The random function has a covariance given by

$$\langle g(t)\, g(s) \rangle = R_g(t-s) = \frac{1}{2\pi} \int_{-\infty}^{\infty} \Psi(\omega)\, e^{i\omega(t-s)}\, d\omega \qquad (1.53)$$

where $R_g(t-s)$ is the autocorrelation function for $g(t)$; it depends only on the time difference $(t-s)$, and not on t and s individually.

The covariances of both the velocity (Eq. 1.51) and the acceleration (Eq. 1.52), are given by

$$\langle \dot{f}(t)\, \dot{f}(s) \rangle = (e^{-\alpha t} - e^{-\beta t})\, (e^{-\alpha s} - e^{-\beta s})\, \langle g(t)\, g(s) \rangle \quad , \qquad (1.54)$$

and

$$\begin{aligned} \langle \ddot{f}(t)\, \ddot{f}(s) \rangle = {} & (-\alpha e^{-\alpha t} + \beta e^{-\beta t})\, (-\alpha e^{-\alpha s} + \beta e^{-\beta s})\, \langle g(t)\, g(s) \rangle \\ & + (-\alpha e^{-\alpha t} + \beta e^{-\beta t})(e^{-\alpha s} - e^{-\beta s})\, \langle g(t)\, \dot{g}(s) \rangle \\ & + (e^{-\alpha t} - e^{-\beta t})(-\alpha e^{-\alpha s} + \beta e^{-\beta s})\, \langle \dot{g}(t)\, g(s) \rangle \\ & + (e^{-\alpha t} - e^{-\beta t})(e^{-\alpha s} - e^{-\beta s})\, \langle \dot{g}(t)\, \dot{g}(s) \rangle \end{aligned} \qquad (1.55)$$

in which

$$\begin{aligned} \langle \dot{g}(t)\, g(s) \rangle = -\langle g(t)\, \dot{g}(s) \rangle = \dot{R}_g(t-s) = \frac{i}{2\pi} \int_{-\infty}^{\infty} \omega\, \Psi(\omega)\, e^{i\omega(t-s)}\, d\omega \\ - \langle \dot{g}(t)\, \dot{g}(s) \rangle = \ddot{R}_g(t-s) = -\frac{1}{2\pi} \int_{-\infty}^{\infty} \omega^2 \Psi(\omega)\, e^{i\omega(t-s)}\, d\omega \end{aligned} \qquad (1.56)$$

Now, substitution of Eqs. 1.47, 1.53, 1.54, 1.55 and 1.56 into

Eq. 1.48, after lengthy algebra operations, yields

$$\langle \eta_n^2(t) \rangle = \left(\frac{4}{n\pi}\right)^2 \frac{1}{2\pi} \int_{-\infty}^{\infty} \Psi(\omega) \Big[|J_n(\omega, t; \alpha, \beta)|^2 + 2\omega \, \mathrm{Im}\{J_n(\omega, t; \alpha, \beta) \, \overline{J}_n(\omega, t; 1, 1)\} + \omega^2 |J_n(\omega, t; 1, 1)|^2 \Big] d\omega , \tag{1.57}$$

where $\overline{J}_n$ denotes the complex conjugate of J_n. The expressions for $J_n(\omega, t; 1, 1)$ are shown in Appendix I-a.

For the purpose of numerical computation, Shinozuka [1] suggested the following power spectrum

$$\Psi(\omega) = De^{-B^2\omega^2} , \tag{1.58}$$

where B and D are constants. Shinozuka admits that the applicability of this form of $\Psi(\omega)$ to earthquake problems is open to question; however, due to the lack of statistical studies concerning earthquake ground displacement, a superior spectrum has not been discovered by this investigation. The autocorrelation function of Eq. 1.58 is

$$R_g(\tau) = \left(\frac{D}{2\sqrt{\pi}\, B}\right) e^{\left(\frac{-\tau^2}{4B^2}\right)} . \tag{1.59}$$

Expressing all the parameters in nondimensional form enables one to visualize some of the characteristics of the problem. By introducing ω_1 from Eq. 1.21, one can obtain the dimensionless quantities

$$\left.\begin{aligned} \overset{*}{t} &= \omega_1 t \quad , \quad \overset{*}{\omega} = \frac{\omega}{\omega_1} \quad , \quad \overset{*}{\omega}_n = \frac{\omega_n}{\omega_1} = n \quad , \\ \overset{*}{\omega}_{dn} &= \frac{\omega_{dn}}{\omega_1} = n\sqrt{1-\xi_n^2} \quad , \quad \overset{*}{\alpha} = \frac{\alpha}{\omega_1} \text{ and } \overset{*}{\beta} = \frac{\beta}{\omega_1} \end{aligned}\right\} , \qquad (1.60)$$

and

$$\overset{*}{\Psi}(\overset{*}{\omega}) = \frac{\Psi(\omega)}{D} = \frac{\Psi(\omega_1 \overset{*}{\omega})}{D} = e^{-B^2\omega_1^2\overset{*}{\omega}^2} . \qquad (1.61)$$

Therefore, Eq. 1.57 becomes

$$\langle \eta_n^2(t) \rangle = \left(\frac{4}{n\pi}\right)^2 \frac{D}{2\pi} \sqrt{\frac{\rho}{Gk'}} \frac{L}{\pi} \int_{-\infty}^{\infty} e^{-B^2\omega_1^2\overset{*}{\omega}^2} \left[\left| \overset{*}{J}_n(\overset{*}{\omega}, \overset{*}{t}; \overset{*}{\alpha}, \overset{*}{\beta}) \right|^2 + \right.$$

$$\left. + 2\overset{*}{\omega}\, \mathrm{Im}\{\overset{*}{J}_n(\overset{*}{\omega}, \overset{*}{t}; \overset{*}{\alpha}, \overset{*}{\beta})\, \overline{\overset{*}{J}}_n(\overset{*}{\omega}, \overset{*}{t}; 1, 1)\} + \overset{*}{\omega}^2 \left| \overset{*}{J}_n(\overset{*}{\omega}, \overset{*}{t}; 1, 1) \right|^2 \right] d\overset{*}{\omega} . \qquad (1.62)$$

Upon using the modal solution $v(x, t) = \sum_{n=1, 3, 5}^{\infty} \Phi_n(x)\, \eta_n(t)$, one can obtain the mean square displacement as

$$\langle v^2(x, t) \rangle = \sum_{n=1, 3, 5}^{\infty} \sin^2 \frac{n\pi x}{L} \langle \eta_n^2(t) \rangle . \qquad (1.63)$$

Evaluating the integral of Eq. 1.62 is very involved; so its value was obtained numerically by using the Hildebrand algorithm, which is based on the following relation

$$\int_{-\infty}^{\infty} e^{-\lambda^2 x^2} f(x)\, dx = \frac{\sqrt{\pi}}{6\lambda} \left[f\left(-\frac{\sqrt{6}}{2\lambda}\right) + 4f(0) + f\left(\frac{\sqrt{6}}{2\lambda}\right) \right] \qquad (1.64)$$

A numerical example is presented for the set of parameters $\overset{*}{\alpha}$ and $\overset{*}{\beta}$, i.e., for different envelope functions as shown in Fig. I-14 where four types, designated by A, B, C and D, are as follows:

Type	$\overset{*}{\alpha}$	$\overset{*}{\beta}$
A	0.2	0.5
B	0.5	1.0
C	0.8	1.5
D	2.0	4.0

The corresponding mean square displacement $(\overset{*}{v})^2$ was plotted in Fig. I-15, where

$$(\overset{*}{v})^2 = \frac{\langle v^2(x, \overset{*}{t})\rangle}{DL\sqrt{\frac{\rho}{k'G}}} \qquad (I.65)$$

Only the first term of the series of Eq. 1.63 was considered because the series is rapidly convergent.

In the numerical example, the damping was taken to be 10%, which is quite high, and the quantity $B^2\omega_1^2$ in the power spectrum was taken equal to 0.5.

It is important to note, also, that the contribution from the term $\sin^2 \frac{n\pi x}{L}$ in Eq. 1.63 was taken to be equal to $\frac{1}{2}$ indicating one of two possibilities

1. $x = \frac{L}{4}$ or $\frac{3L}{4}$, or

2. the space average of the mean square displacement is in the form

$$\langle \widetilde{v^2(x, t^*)} \rangle = \sum_{n=1, 3, 5}^{\infty} \frac{1}{L} \int_0^L \sin^2 \frac{n\pi x}{L} \, dx \, \langle \eta_n^2(t^*) \rangle \quad . \qquad (1.66)$$

Figs. I-14 and I-15 show the correlation between the shape of the envelope function G(t) and the corresponding mean square displacement $(\overset{*}{v})^2$. In all curves of Fig. I-15, there is a rapid decaying of these response curves due to the high percentage of damping which has been assumed (10%).

I-3-3. Dynamic response under random accelerations

Another example of random excitation is based on the random acceleration with specific duration, which is given as

$$F(t) = [H(t) - H(t - t_0)] \ddot{g}(t) \quad , \qquad (1.67)$$

where H(t) is the unit step function (the Heaviside function), and t_0 is the duration of this input excitation. The displacements both during and after the application of the random acceleration are presented.

The solution of Eq. 1.45, which is in the form of Eq. 1.48, may be reduced to the following form, after much algebra is performed

$$\langle \eta_n^2(t) \rangle = \frac{1}{2\pi} [H(t) - H(t - t_0)] \left(\frac{4}{n\pi} \right)^2 \int_{-\infty}^{\infty} \Psi(\omega) I(\omega, t) \, d\omega \quad ; \qquad (1.68)$$

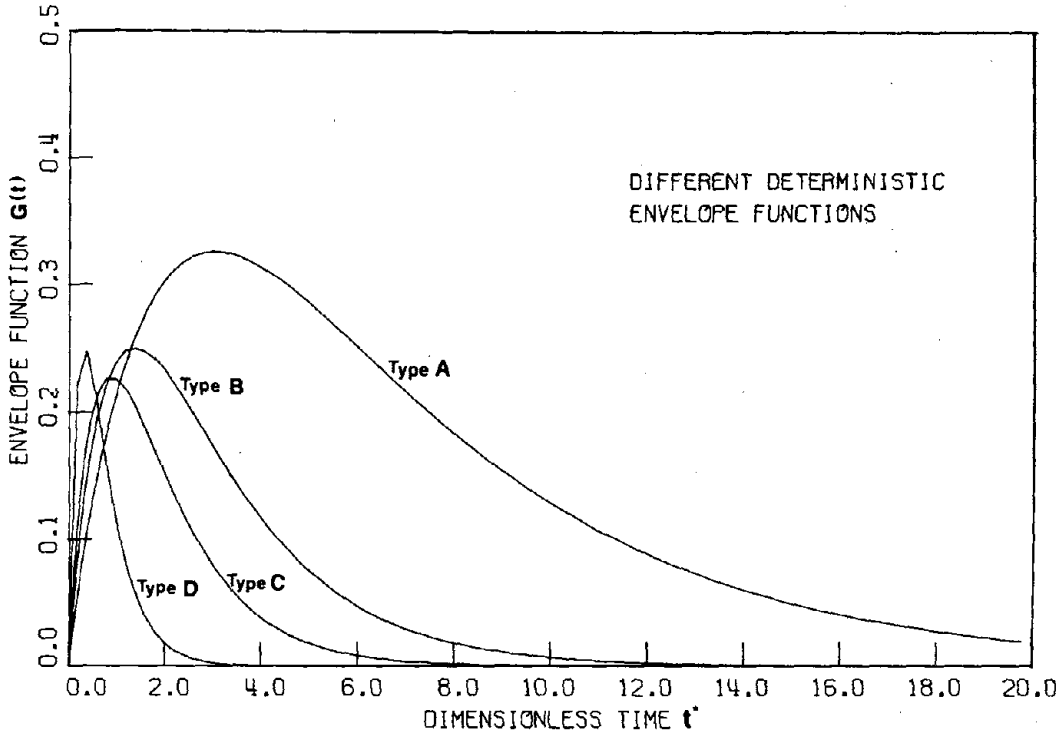

Fig. I-14

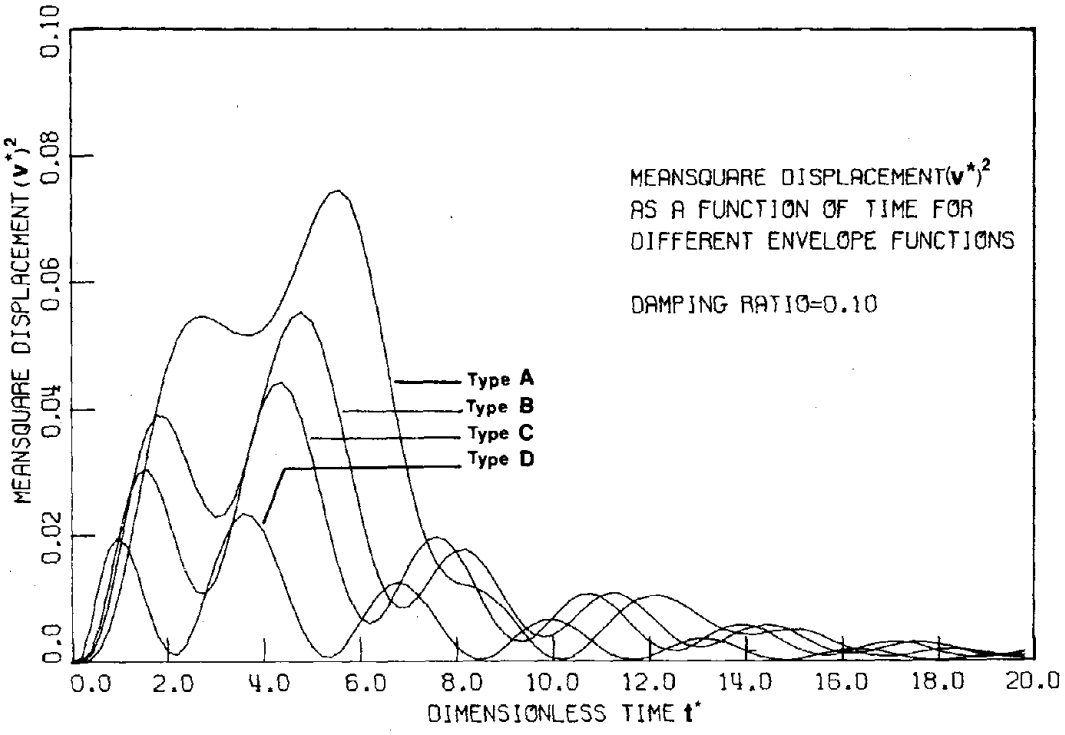

Fig. I-15

the expression for $I(\omega, t)$ is given in Appendix I-b.

Another method to evaluate the integral of Eq. 1.68, is the one suggested by Caughey and Stumpf[2]; their method approximates the integral of Eq. 1.68 by

$$\langle \eta_n^2(t) \rangle \simeq \frac{\Psi(\omega_{dn})}{2\pi} [H(t) - H(t - t_0)] \left(\frac{4}{n\pi}\right)^2 \left[\int_{-\infty}^{\infty} I(\omega, t)\, d\omega \right] , \qquad (1.69)$$

which, with the aid of Appendix I-b, becomes

$$\langle \eta_n^2(t) \rangle \simeq \frac{\Psi(\omega_{dn})}{2\pi} [H(t) - H(t - t_0)] \left(\frac{4}{n\pi}\right)^2 \frac{1}{\xi_n} \left[1 - e^{-2\xi_n \omega_n t} + \xi_n^2 \left(e^{-2\xi_n \omega_n t} \cos 2\omega_{dn} t - \frac{\sqrt{1 - \xi_n^2}}{\xi_n} e^{-2\xi_n \omega_n t} \sin 2\omega_{dn} t - 1 \right) \right] . \qquad (1.70)$$

The power spectral density of strong motion earthquake acceleration suggested by Tajima[8] was used for the purpose of numerical computation. The power spectrum [7] is in the form

$$\Psi(\omega) = \frac{0.01238 \left(1 + \frac{\omega^2}{147.8}\right)}{\left(1 - \frac{\omega^2}{242}\right)^2 + \left(\frac{\omega^2}{147.8}\right)} . \qquad (1.71)$$

The root mean square (rms) value of the displacement was computed for the random input, for different durations of the excitation (t_0 = 30, 20 and 10 seconds). Also, the free vibrational displacement which followed the forced vibration was computed. The time history of the two displacements is shown in Figs. I-16 and I-17, where only two terms of the series of Eq. 1.63 were considered. In these figures,

ω_1 (the fundamental frequency) was assumed to be 0.3 rad/sec.; i.e., the natural period was taken to be about 21 sec., which is the fundamental period of a long-span suspension bridge. The damping was taken to be 10% which is, again, a very high value. The figures show the displacement at the mid-point of the span; for the displacement at $\frac{L}{4}$ and $\frac{3L}{4}$, or for the space average of the displacement, one has to multiply the ordinate by 0.707.

As is seen from Figs. I-16 and I-17, for the 30 seconds duration, the displacement at the mid-point of the beam reaches a value of 1.7 ft. at $t \simeq 33$ sec., while for 10 seconds duration, the displacement reduces to 1.2 ft. at about 13 seconds. One can notice, also, that the maximum displacement always occurs immediately after the excitation subsides.

Fig. I-18 shows the energy content of the system with both the strain and kinetic energies plotted for the example of 30 seconds duration. The figure demonstrates the gradual increase of the two energies during the input motion; subsequently, during free vibration, the kinetic energy is at its minimum when the strain energy is at its maximum. The sum of the two energies is the envelope of the two curves, and it is shown in the same figure.

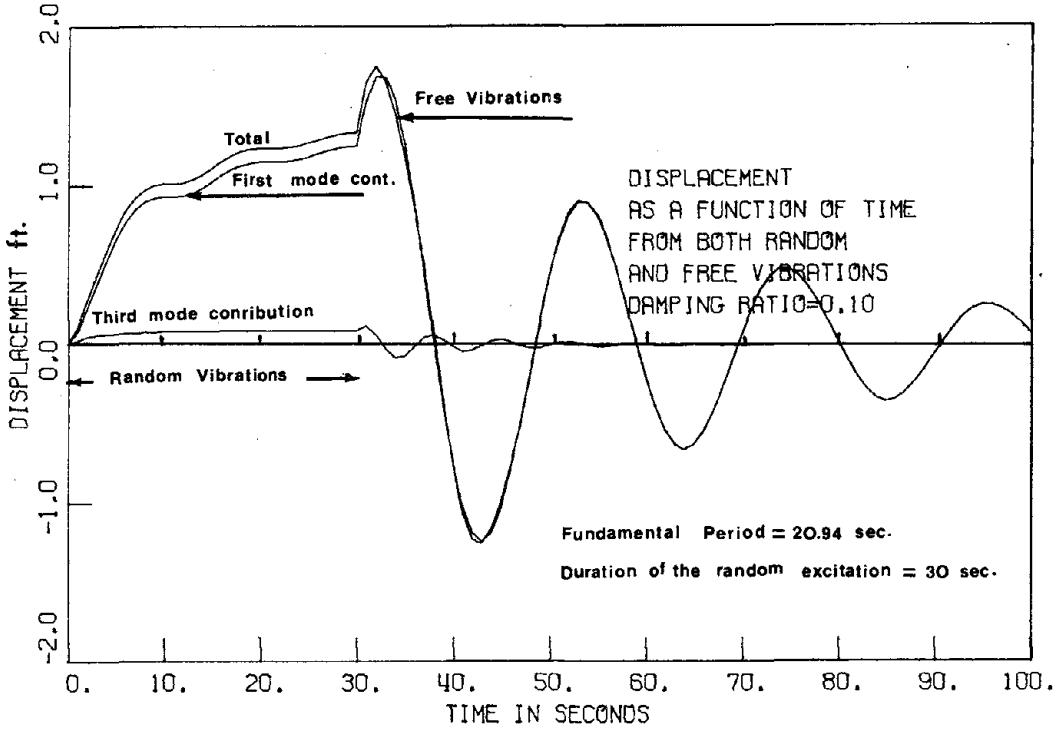

Fig. I-16

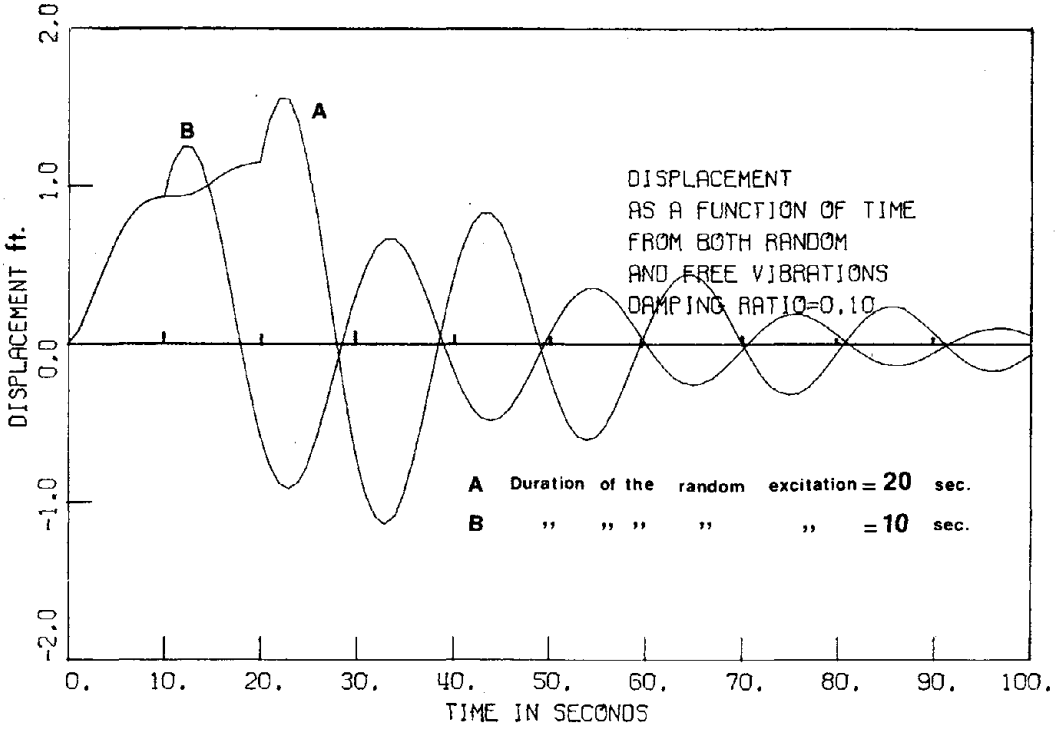

Fig. I-17

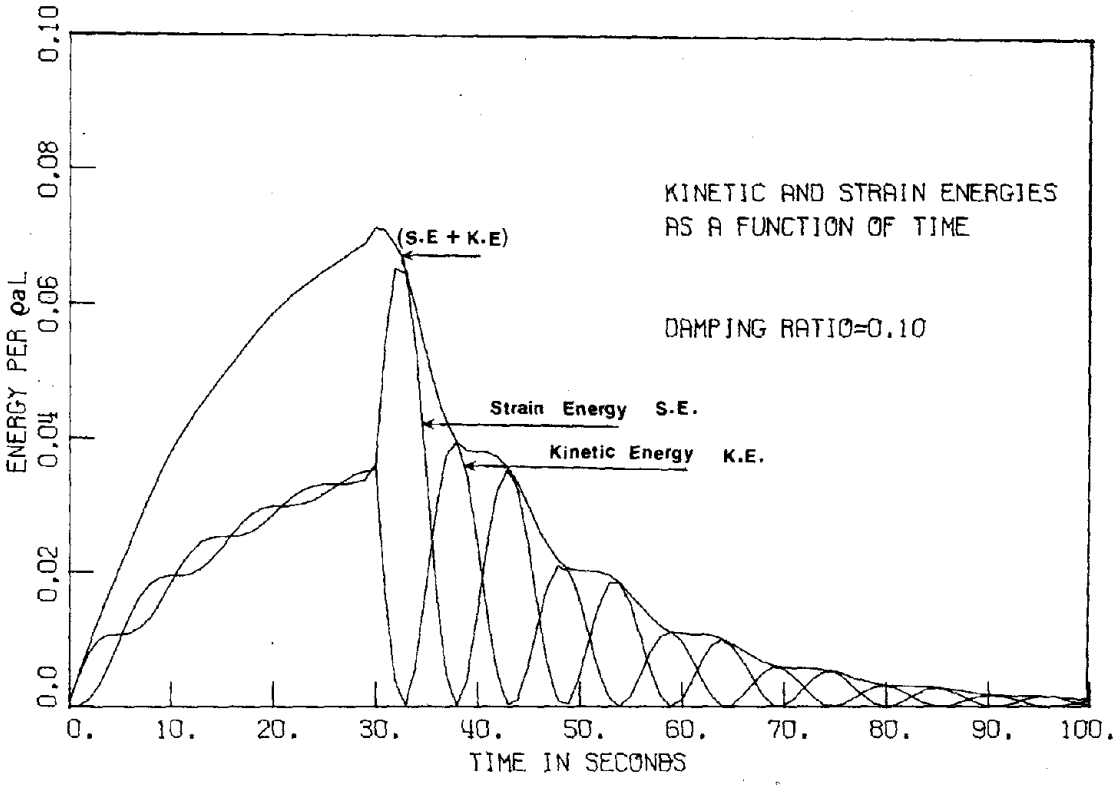
KINETIC AND STRAIN ENERGIES
AS A FUNCTION OF TIME
DAMPING RATIO=0.10
(S.E + K.E)
Strain Energy S.E.
Kinetic Energy K.E.
ENERGY PER ρaL
0.0
0.02
0.04
0.06
0.08
0.10
0.
10.
20.
30.
40.
50.
60.
70.
80.
90.
100.
TIME IN SECONDS

Fig. I-18

I-4. Conclusions

This study has examined the effect when the two end supports of a simply supported uniform bridge deck (assumed to be shear beam type) are shaken simultaneously by earthquake-type motion; this situation was analyzed in both the frequency and time domains, with harmonic and random excitations, respectively.

In the harmonic vibration analysis, the response of the beam as well as the correlation between the two support-point excitations have been investigated. The different modes of vibration are related to the nature of the support movement; in particular, they depend on the relative phase of the two support motions. When the two supports move in phase, symmetric modes of beam vibration can be excited, while when the end supports are moving 180° out of phase, the anti-symmetric modes are excited.

In the random vibration analysis, two methods are presented to determine the stochastic response of the beam when it is subjected to identical stationary Gaussian excitations acting simultaneously on both end supports. Both methods indicated that significant displacement amplitude occurs immediately subsequent to the end of the random excitations.

I-5. Appendices

Appendix I-a

Expressions for $J_n(\omega, t; \alpha, \beta)$ and $J_n(\omega, t; 1, 1)$

The complex quantities $J_n(\omega, t; \alpha, \beta)$ and $J_n(\omega, t; 1, 1)$ of Eq. 1.58 are given by

$$J_n(\omega, t; \alpha, \beta) = \int_0^t h(t-\tau)(\alpha e^{-\alpha\tau} - \beta e^{-\beta\tau})\, e^{i\omega\tau}\, d\tau \quad ,$$

and

$$J_n(\omega, t; 1, 1) = \int_0^t h(t-\tau)(e^{-\alpha\tau} - e^{-\beta\tau})\, e^{i\omega\tau}\, d\tau \quad .$$

Let $G_n(\omega, t; \theta)$ and $H_n(\omega, t; \theta)$ be defined as

$$G_n(\omega, t; \theta) = \mathrm{Re}\left\{\int_0^t h(t-\tau)\, e^{(-\theta + i\omega)\tau}\, d\tau\right\}$$

and

$$H_n(\omega, t; \theta) = \mathrm{Im}\left\{\int_0^t h(t-\tau)\, e^{(-\theta + i\omega)\tau}\, d\tau\right\}$$

where θ stands for α and β .

Then, $J_n(\omega, t; \alpha, \beta)$ and $J_n(\omega, t; 1, 1)$ can be written as

$$J_n(\omega, t; \alpha, \beta) = [\alpha G_n(\omega, t; \alpha) - b\, G_n(\omega, t; \beta)] + i[\alpha H_n(\omega, t; \alpha) - \beta H_n(\omega, t; \beta)]$$

and

$$J_n(\omega, t; 1, 1) = [G_n(\omega, t; \alpha) - G_n(\omega, t; \beta)] + i[H_n(\omega, t; \alpha) - H_n(\omega, t; \beta)]$$

$G_n(\omega, t; \theta)$ and $H_n(\omega, t; \theta)$ are evaluated and given by

$$G_n(\omega, t;\theta) = \frac{1/\omega_{dn}}{\left[(\xi_n\omega_n-\theta)^2+\omega_{dn}^2-\omega_n^2\right]^2+4\omega^2(\xi_n\omega_n-\theta)^2}\left[\left\{(\omega_n\xi_n-\theta)^2+\omega_{dn}^2-\omega^2\right\}\cdot\right.$$

$$\left\{\omega_{dn}e^{-\theta t}\cos\omega t - (\xi_n\omega_n-\theta)e^{-\xi_n\omega_n t}\sin\omega_{dn}t-\omega_{dn}e^{-\xi_n\omega_n t}\cos\omega_{dn}t\right\}$$

$$\left. + 2\omega(\xi_n\omega_n-\theta)\left\{\omega_{dn}e^{-\theta t}\sin\omega t - \omega e^{-\xi_n\omega_n t}\sin\omega_{dn}t\right\}\right]$$

and

$$H_n(\omega, t;\theta) = \frac{1/\omega_{dn}}{\left[(\xi_n\omega_n-\theta)^2+\omega_{dn}^2-\omega^2\right]^2+4\omega^2(\xi_n\omega_n-\theta)^2}\left[\left\{(\omega_n\xi_n-\theta)^2+\omega_{dn}^2-\omega^2\right\}\cdot\right.$$

$$\left\{\omega_{dn}e^{-\theta t}\sin\omega t - \omega e^{-\xi_n\omega_n t}\sin\omega_{dn}t\right\} - 2\omega(\xi_n\omega_n-\theta)\left\{\omega_{dn}e^{-\theta t}\cos\omega t\right.$$

$$\left.\left. - (\xi_n\omega_n-\theta)e^{-\xi_n\omega_n t}\sin\omega_{dn}t - \omega_{dn}e^{-\xi_n\omega_n t}\cos\omega_{dn}t\right\}\right] \quad ;$$

again $\omega_{dn} = \sqrt{1-\xi_n^2}\ \omega_n$ is the damped frequency for the n^{th} mode.

Appendix I-b

Expression for $I(\omega, t)$

$I(\omega, t)$ of Eq. 1.69 can be written, in terms of the unit-impulse-response function $h(t)$ (Eq. 1.48), as

$$I(\omega, t) = \frac{1}{\omega_{dn}^2} e^{-2\xi_n\omega_n t} \int_0^t \int_0^t e^{(\xi_n\omega_n + i\omega)\tau} \sin\omega_{dn}(t-\tau) \cdot e^{(\xi_n\omega_n - i\omega)\tau'} \sin\omega_{dn}(t - \tau') \, d\tau \, d\tau'$$

or, more conveniently, as

$$I(\omega, t) = \frac{1}{\omega_{dn}^2} I_1 \cdot \overline{I}_1$$

where $\overline{I}_1$ denotes the complex conjugate of I_1 which is given by

$$I_1 = \frac{(\omega_n\xi_n)^2 + \omega_{dn}^2 - \omega^2 - 2i\omega\xi_n\omega_n}{\left[(\xi_n\omega_n)^2 + \omega_{dn}^2 - \omega^2\right]^2 + 4(\omega\xi_n\omega_n)^2} \left[\left(\omega_{dn}\cos\omega t - \xi_n\omega_n e^{-\xi_n\omega_n t}\sin\omega_{dn}t - \omega_{dn}e^{-\xi_n\omega_n t}\cos\omega_{dn}t\right) + i\left(\omega_{dn}\sin\omega t - \omega e^{-\xi_n\omega_n t}\sin\omega_{dn}t\right)\right] .$$

Therefore, the expression for $I(\omega, t)$ is

$$I(\omega, t) = \frac{1}{\left[\left(\xi_n\omega_n\right)^2+\omega_{dn}^2-\omega^2\right]^2+4\left(\xi_n\omega_n\omega\right)^2}\left[1+e^{-2\xi_n\omega_n t}\left(1+\frac{\left(\xi_n\omega_n\right)^2-\omega_{dn}^2}{\omega_{dn}^2}\sin^2\omega_{dn}t\right.\right.$$

$$\left.+2\xi_n\frac{\omega_n}{\omega_{dn}}\sin\omega_{dn}t\ \cos\omega_{dn}t\right)+e^{-2\xi_n\omega_n t}\frac{\omega^2}{\omega_{dn}^2}\sin^2\omega_{dn}t$$

$$+2e^{-\xi_n\omega_n t}\left(-\cos\omega_{dn}t-\frac{\xi_n\omega_n}{\omega_{dn}}\sin\omega_{dn}t\right)\cos\omega t$$

$$\left.-2e^{-\xi_n\omega_n t}\frac{\omega}{\omega_{dn}}\sin\omega_{dn}t\sin\omega t\right] \quad .$$

REFERENCES OF CHAPTER I

1. Shinozuka, M. and Henry, L., "Random Vibration of a Beam Column," Journal of Engineering Mechanics Division, Proceedings of the American Society of Civil Engineers, EM 5, October 1965, pp. 123-143.

2. Caughey, T.K. and Stumpf, H.J., "Transient Response of a Dynamic System under Random Excitation," Journal of Applied Mechanics, Transactions of the American Society of Mechanical Engineers, Vol. 28, December 1961, pp. 563-566.

3. Bogdanoff, J.L., Goldberg, J.E. and Bernard, M.C., "Response of a Simple Structure to a Random Earthquake-Type Disturbance," Bulletin of the Seismological Society of America, Vol. 91, 1961, pp. 293-310.

4. Bolotin, V.V., "Statistical Theory of the Aseismic Design of Structures," Proceedings of the Second World Conference on Earthquake Engineering, Japan, Vol. II, 1960, pp. 1365-1374.

5. Rosenblueth, E. and Bustamante, J.L., "Distribution of Structural Response to Earthquakes," Journal of Engineering Mechanics Division, Proceedings of the American Society of Civil Engineers, Vol. 88, EM 3, June 1962, pp. 75-106.

6. Goldberg, J.E., Bogdanoff, J.L. and Sharpe, D.R., "The Response of Simple Nonlinear Systems to a Random Disturbance of the Earthquake Type," Bulletin of the Seismological Society of America, Vol. 54, No. 1, February 1964, pp. 263-276.

7. Housner, G.W. and Jennings, P.C., "Generation of Artificial Earthquakes," Journal of Engineering Mechanics Division, Proceedings of the American Society of Civil Engineers, Vol. 90, EM 1, February 1964, pp. 113-150.

8. Tajima, H., "A Statistical Method of Determining the Maximum Response of a Building Structure During an Earthquake," Proceedings of the Second World Conference on Earthquake Engineering, Tokyo and Kyoto, Japan, Vol. II, July 1960.

9. Kanai, K., "Semi-Empirical Formula for the Seismic Characteristics of the Ground," Bulletin of the Earthquake Research Institute, University of Tokyo, Tokyo, Japan, Vol. 35, June 1957, pp. 309-325.

CHAPTER II

ANTIPLANE DYNAMIC SOIL-BRIDGE INTERACTION FOR INCIDENT PLANE SH-WAVES

II-1. Introduction

The problem of the dynamic interaction between buildings and the soil during earthquake excitation has attracted considerable interest of many investigators [1, 2, 3, 4, 5]. However, such analyses have, so far, not been extended to more complicated structures, such as bridges or large industrial buildings, where differential motions of foundations might influence response in an important way, as seen in Chapter I.

There have been many cases reported in the literature in which bridges suffered damage during earthquakes [6, 7]. These examples clearly indicate the need for detailed investigations of the dynamic soil-bridge interaction to determine the significance of that interaction on the bridge response. The soil-bridge interaction effect is considered important, for example, when the motion of an abutment or foundation is significantly different from the motion of the ground in the absence of the bridge, the latter motion being usually referred to as the free-field ground motion.

The general dynamic soil-structure interaction problem can be broken down into three parts [8]. These are:

1. The determination of the input motion to the foundations (the contribution of the seismic waves) or equivalently the determination of the driving forces.
2. The evaluation of the force-displacement relationship (the impedance functions or their reciprocal, the compliance functions) for the foundations.
3. The solution of the equations of motion including both the foundations and the superstructure.

This approach has the advantage that once the solutions of the first two parts have been obtained for a class of foundations, the results can be used to calculate the interaction response of different structures. This is done by superimposing the results so that the equations of motion for the foundations are satisfied. This method, of course, is possible only if the problem is linear.

Luco and Contesse [5] have studied the dynamic interaction, through the soil for two parallel infinite shear walls placed on rigid foundations and for vertically incident SH-waves. In a similar study Wong and Trifunac [9] have determined the driving forces induced by harmonic plane SH-waves and the impedance functions for a class of embedded foundations with circular cross sections at different separation distances. These results will be used in the present analysis of a two-dimensional superstructure (the girder), the substructure (the two abutments) and the two foundations.

In the following study, the analysis of dynamic soil-bridge interaction has been performed in three steps. These are:

1. the analysis of input motions
2. the force-displacement relationships for the foundations
3. the dynamic analysis of the structure itself, i.e., the bridge.

Based on the exact solution of the first two steps, the dynamic interaction of a simple two-dimensional bridge model erected on the elastic half-space has been investigated for a single span case. The two-dimensional model under study consists of an elastic shear girder bridge supported by two rigid abutments and rigid foundations which have a circular cross section and are welded to the half-space. It has been shown that the dynamic interaction depends on:

1. the incidence angle of plane SH-waves,
2. the ratio of the rigidity of the girder and the soil,
3. the ratio of the girder mass to the mass of the rigid abutment-foundation system, and
4. the span of the bridge.

The dynamic response of the girder and the effect of the radiative damping in the half-space on the interaction of the girder have been studied.

Finally, the model considered in this study offers obvious analytical advantages and a simple and direct insight into a complicated wave propagation phenomenon. However, this model represents a highly simplified version of the actual three-dimensional problem, in which in-plane as well as anti-plane incident waves are present, and

where coupling between the horizontal, rocking, torsional and vertical motions of the structure and the foundations take place.

II-2. The Model, the Excitation and the Exact Solution

The two-dimensional model studied in this analysis is shown in Fig. II-1-a. It consists of three structural elements: the superstructure (the girder), the substructure (the abutments) and the foundations. These elements are assumed to be infinitely extended in the z-direction. Furthermore, the following assumptions are made:

1. The soil, which is represented by the half-space, is elastic, isotropic and homogeneous. Its rigidity and the velocity of shear waves are μ_s and β_s, respectively.
2. The two foundations are assumed to be rigid, semicircular in cross section, and welded to the half-space.
3. The abutments are also assumed to be rigid. They are welded to the foundations so they behave together as a rigid body partially embedded in the soil.
4. The model for the girder is a shear beam, of span L and depth d, supported at the ends by the rigid piers. The beam is isotropic and homogeneous; the rigidity and the velocity of the shear waves in the beam are given by μ_b and β_b, respectively.

II-2-1. The coordinate systems

1. For the superstructure, i.e., the girder, the origin of x and y coordinates is located at the left support point as shown in Fig. II-1-a. The x-axis is defined along the span of the bridge, while the y-axis is in the vertical direction.

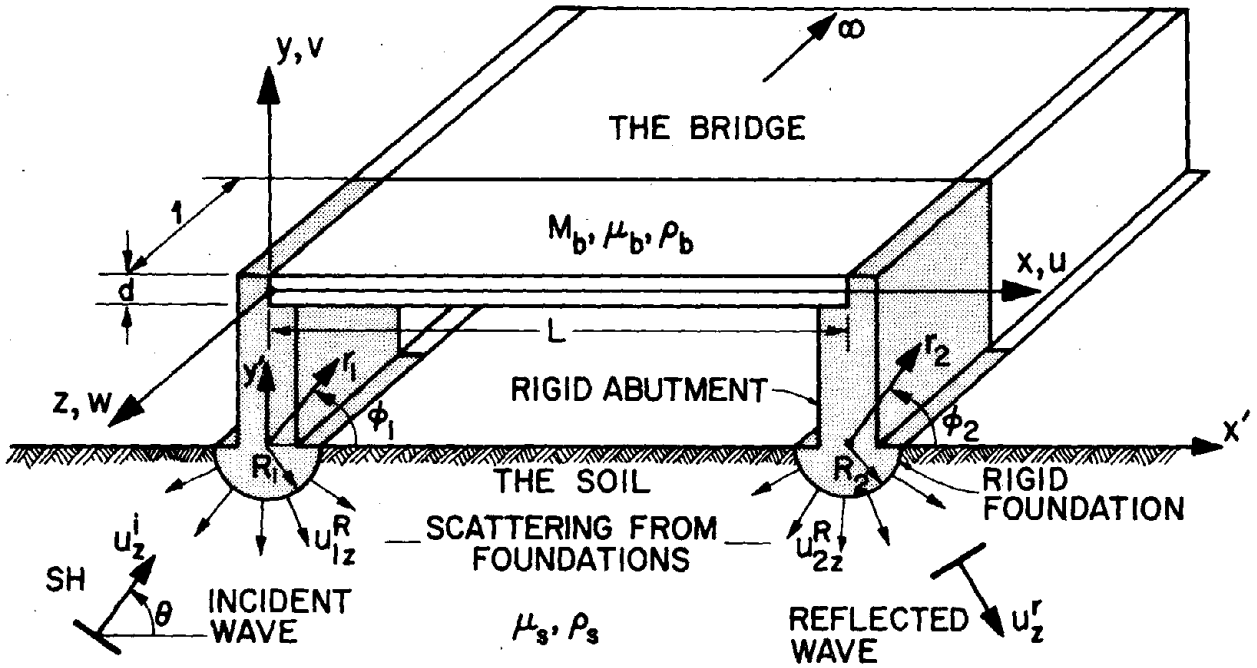
y, v
∞
THE BRIDGE
M_b, μ_b, ρ_b
x, u
t
d
L
z, w
y'
r_1
ϕ_1
RIGID ABUTMENT
r_2
ϕ_2
x'
R_1
R_2
THE SOIL
RIGID FOUNDATION
u_z^i
u_{1z}^R
SCATTERING FROM FOUNDATIONS
u_{2z}^R
SH
θ
INCIDENT WAVE
μ_s, ρ_s
REFLECTED WAVE
u_z^r

(a)

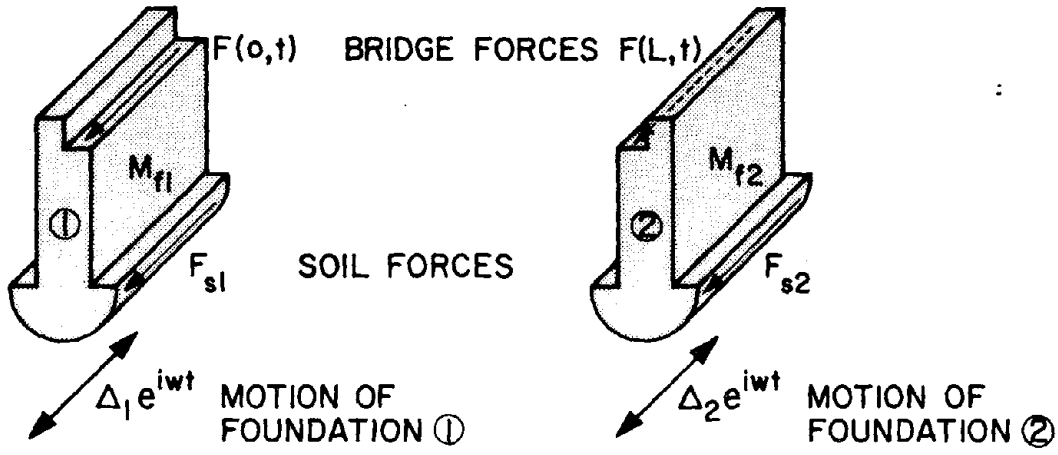
F(o,t)
BRIDGE FORCES F(L,t)
M_{f1}
①
F_{s1}
SOIL FORCES
M_{f2}
②
F_{s2}
$\Delta_1 e^{iwt}$
MOTION OF FOUNDATION ①
$\Delta_2 e^{iwt}$
MOTION OF FOUNDATION ②

(b)

Fig. II-1

2. For the two rigid abutment-foundation systems, the scattered waves from the two rigid foundations are best represented by polar coordinates (r_1, φ_1) and (r_2, φ_2), which have their origins at the center of each foundation. The cartesian coordinates (x', y') are located at the left foundation such that

$$\begin{Bmatrix} x_1 \\ x_2 \end{Bmatrix} = \begin{Bmatrix} x' \\ x' - L \end{Bmatrix} = \begin{Bmatrix} r_1 \cos\varphi_1 \\ r_2 \cos\varphi_2 \end{Bmatrix} , \quad \begin{Bmatrix} y_1 \\ y_2 \end{Bmatrix} = \begin{Bmatrix} r_1 \sin\varphi_1 \\ r_2 \sin\varphi_2 \end{Bmatrix} . \tag{2.1}$$

This choice of the (r_1, φ_1) and (r_2, φ_2) coordinate systems is identical to that used by Wong and Trifunac [9].

As shown by several investigators [5, 9, 10], the interaction problem can be separated into three steps:

1. Input motion or "driving forces."
2. Impedance functions or "compliance functions."
3. Dynamic analysis of the structure (bridge).

The final results are then obtained by superposition. Some parts of these analyses are given in this study for the completeness of this presentation, as follows.

II-2-2. Motion of the soil

It is assumed that the excitation is in a form of plane harmonic SH-waves with an amplitude equal to one and with the angle of incidence θ, which is measured counterclockwise from the horizontal axis to the normal on the plane wave front (Fig. II-1-a). This incident wave is given by

$$u_z^i(x', y', t) = e^{i\omega(t - x'/c_x - y'/c_y)} \quad , \tag{2.2}$$

where

$$c_x = \frac{\beta_s}{\cos\theta} \quad , \quad c_y = \frac{\beta_s}{\sin\theta} \quad , \tag{2.3}$$

and $\beta_s = \sqrt{\frac{\mu_s}{\rho_s}}$ ... is the shear wave velocity in the soil; μ_s is the shear modulus of the soil, and ρ_s is the density.

The resulting free-field motion, i.e., motion of the half-space in the absence of the bridge and its foundations, becomes

$$u_z^{i+r}(x', y', t) = 2\, e^{i\omega t}\left[e^{-i\frac{\omega}{\beta_s} x' \cos\theta}\right] \cos\left(\frac{\omega y'}{\beta_s} \sin\theta\right) \quad , \tag{2.4}$$

where u_z^{i+r} stands for the sum of incident, u_z^i, and reflected, u_z^r, waves from the half-space boundary $y' = 0$. This motion can be represented in terms of polar coordinates (r_1, φ_1) and (r_2, φ_2) [9].

The total displacement field u_z, in the half-space in the presence of the two rigid foundations is composed of the free-field motion u_z^{i+r} and the scattered waves, u_{1z}^R and u_{2z}^R, from the two foundations; i.e.,

$$u_z = u_z^{i+r} + u_{1z}^R + u_{2z}^R \quad . \tag{2.5}$$

This total displacement, u_z, must satisfy the Helmholtz equation in each of the (r_1, φ_1) and (r_2, φ_2) coordinate systems

$$\frac{\partial^2 u_z}{\partial r_j^2} + \frac{1}{r_j}\frac{\partial u_z}{\partial r_j} + \frac{1}{r_j^2}\frac{\partial^2 u_z}{\partial \varphi_j^2} + k_s^2 u_z = 0 \quad , \quad j = 1, 2 \, , \tag{2.6}$$

in which $k_s = \frac{\omega}{\beta_s}$ is the wave number, and the two boundary conditions:

1. Stress-free surface boundary condition

$$\sigma_{\varphi_j z} = \frac{\mu_s}{r_j} \frac{\partial u_z}{\partial \varphi_j} = 0 \quad \text{at} \quad \varphi_j = -\pi \ , \ 0 \ , \ j = 1, 2, \quad r_j \geq R_j \ , \tag{2.7}$$

2. Harmonic displacement boundary condition

$$u_z(R_j, \varphi_j, t) = \Delta_j e^{i\omega t} \quad , \quad -\pi \leq \varphi_j \leq 0 \quad , \quad j = 1, 2 \ , \tag{2.8}$$

where Δ_1 and Δ_2 are the displacement amplitudes of the two foundations (Fig. II-1-b). Δ_1 and Δ_2 are unknown and depend on the soil-structure interaction of both foundations and on the characteristics of the incoming waves.

This interaction problem can be analyzed in three parts which are illustrated in Fig. II-2-i. This figure represents a generalization of the solution method presented by Wong and Trifunac [9] to the soil-bridge interaction problem studied in this analysis.

II-2-3. Forces generated by the soil and compliance functions

The forces exerted by the soil on the two foundations and caused by the incident waves and the motion of the neighboring foundations, as shown in Fig. II-1-b, are given by

$$\begin{Bmatrix} F_{s1} \\ F_{s2} \end{Bmatrix} = - \begin{Bmatrix} -\int_{-\pi}^{0} \sigma_{rz}(R_1, \varphi_1) R_1 d\varphi_1 \\ -\int_{-\pi}^{0} \sigma_{rz}(R_2, \varphi_2) R_2 d\varphi_2 \end{Bmatrix} \ , \tag{2.9}$$

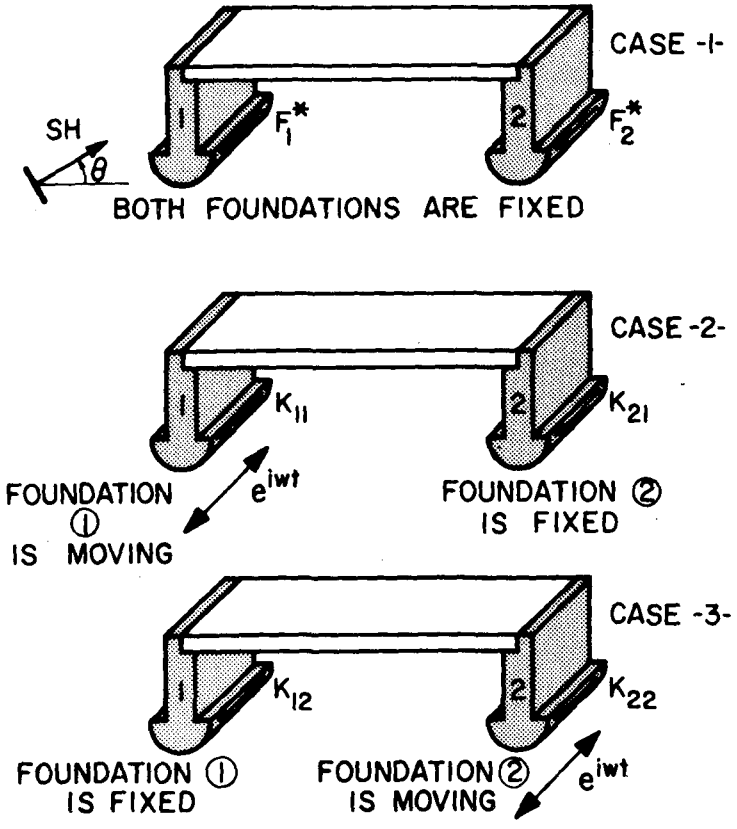
CASE -1-
SH
θ
1
2
F_1^*
F_2^*
BOTH FOUNDATIONS ARE FIXED
CASE -2-
1
2
K_{11}
K_{21}
e^{iwt}
FOUNDATION ① IS MOVING
FOUNDATION ② IS FIXED
CASE -3-
1
2
K_{12}
K_{22}
FOUNDATION ① IS FIXED
FOUNDATION ② IS MOVING
e^{iwt}
FORCES EXERTED BY THE SOIL ON THE TWO FOUNDATIONS

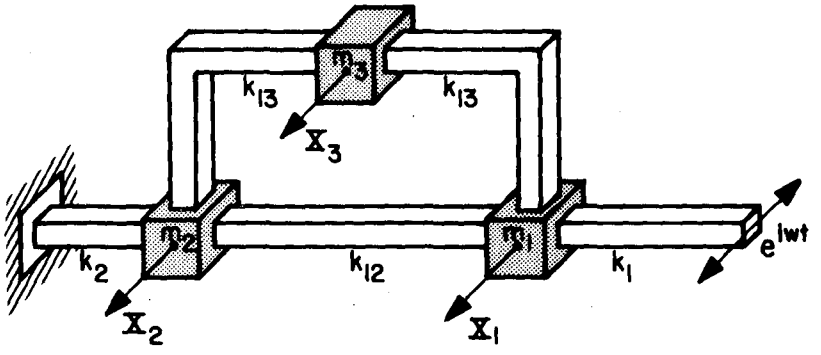
m_3
k_{13}
k_{13}
X_3
m_2
m_1
k_2
k_{12}
k_1
e^{iwt}
X_2
X_1

Fig. II-2

where

$$\sigma_{rz}(R_i, \varphi_i) = \mu_s \left. \frac{\partial u_z}{\partial r_i} \right|_{r_i = R_i} , \quad i = 1, 2 . \tag{2.10}$$

Using the principle of superposition, the total soil forces can be expressed in terms of the "driving forces," and the unknown displacements $\{\Delta\}$ premultiplied by the impedance matrix,

$$\begin{Bmatrix} F_{s1} \\ F_{s2} \end{Bmatrix} = \begin{Bmatrix} -F_1^* \\ -F_2^* \end{Bmatrix} + \begin{bmatrix} K_{11} & K_{12} \\ K_{21} & K_{22} \end{bmatrix} \begin{Bmatrix} \Delta_1 \\ \Delta_2 \end{Bmatrix} . \tag{2.11}$$

Here the driving forces F_1^* and F_2^* are the forces exerted by the soil on the two foundations which are held fixed during excitation by the incident waves u_z^i . The driving forces depend on the properties of the foundations and the soil and also on the nature of the seismic excitation. An element of the impedance matrix K_{ij} $(i, j = 1, 2)$ represents force acting on the motionless i^{th} foundation caused by the unit harmonic motion of the j^{th} foundation. The impedance matrix depends only on the characteristics of the foundations and soil and on the frequency of the motion. Fig. II-2-i illustrates the physical meaning of these force coefficients.

II-3. Dynamic Analysis of the Bridge

II-3-1. Motion of the bridge

The displacements u and v of the two-dimensional bridge model are selected to be zero, while the displacement w depends only on the coordinate x. This displacement must satisfy the equation of motion of an undamped shear beam;

$$\frac{\partial^2 w(x,t)}{\partial x^2} = \frac{1}{\beta_b^2} \frac{\partial^2 w(x,t)}{\partial t^2} \quad , \quad 0 \le x \le L \quad , \tag{2.12}$$

in which $\beta_b = \sqrt{\mu_b/\rho_b}$ ... is the shear wave velocity in the beam; μ_b is the shear modulus of the beam, and ρ_b is the density of the beam.

The boundary conditions for the beam are

$$\begin{Bmatrix} w(o,t) \\ w(L,t) \end{Bmatrix} = \begin{Bmatrix} \Delta_1 \\ \Delta_2 \end{Bmatrix} e^{i\omega t} \quad , \tag{2.13}$$

where Δ_1 and Δ_2 are the unknown complex displacements of the two foundations. The solution of Eq. 2.12, compatible with the boundary conditions given by Eq. 2.13, is

$$w(x,t) = \{[\cos(k_b x) - \cot(k_b L)\sin(k_b x)],\ [\operatorname{cosec}(k_b L)\sin(k_b x)]\} \begin{Bmatrix} \Delta_1 \\ \Delta_2 \end{Bmatrix} e^{i\omega t} \tag{2.14}$$

in which $k_b = \omega/\beta_b$ ... is the wave number in the shear beam. From Eq. 2.14, it is seen that the displacement w(x, t) depends on the instantaneous values of the harmonic boundary conditions.

II-3-2. Forces exerted by the bridge

The end resisting forces, per unit length, acting on the two abutments (Fig. II-1-b) are given by

$$\begin{Bmatrix} F_1^b(t) \\ F_2^b(t) \end{Bmatrix} = \begin{Bmatrix} F(o,t) \\ F(L,t) \end{Bmatrix} = \begin{Bmatrix} d\sigma_{xz}^b(o,t) \\ -d\sigma_{xz}^b(L,t) \end{Bmatrix} = \begin{Bmatrix} -\mu_b d \dfrac{\partial w(o,t)}{\partial x} \\ -\mu_b d \dfrac{\partial w(L,t)}{\partial x} \end{Bmatrix} , \quad (2.15)$$

where d is the depth of the shear beam and σ_{xz}^b is the shear stress in the z-direction.

By using Eqs. 2.14 and 2.15, and by introducing the expression

$$M_b = \rho_b d L \quad , \quad (2.16)$$

which corresponds to the mass of the beam per unit length in the z-direction, these support forces can be written as:

$$\begin{Bmatrix} F_1^b(t) \\ F_2^b(t) \end{Bmatrix} = \begin{bmatrix} -\omega^2 M_b \dfrac{\cot(k_b L)}{(k_b L)} & \omega^2 M_b \dfrac{\operatorname{cosec}(k_b L)}{(k_b L)} \\ \omega^2 M_b \dfrac{\operatorname{cosec}(k_b L)}{(k_b L)} & -\omega^2 M_b \dfrac{\cot(k_b L)}{(k_b L)} \end{bmatrix} \begin{Bmatrix} \Delta_1 \\ \Delta_2 \end{Bmatrix} e^{i\omega t} . \quad (2.17)$$

It is convenient to recall here that the undamped natural frequencies of the simply supported shear beam are given by

$$\omega_n = \frac{n\pi}{L}\sqrt{\frac{\mu_b}{\rho_b}} = \frac{n\pi}{L}\beta_b \quad , \quad n = 1, 2, 3, \ldots \quad (2.18)$$

This corresponds to

$$k_b L = n\pi , \quad n = 1, 2, 3, \ldots \tag{2.19}$$

The mode shapes are given by

$$W_n(x) = \sin \frac{n\pi x}{L} , \quad n = 1, 2, 3, \ldots \tag{2.20}$$

II-4. Dynamic Soil-Bridge-Soil Interaction

The unknown foundation displacement amplitudes Δ_1 and Δ_2 can now be determined from the balance of forces exerted on each foundation. These forces are:

1. Soil forces F_{s1} and F_{s2}, as given by Eq. 2.11.
2. Bridge end forces $F_1^b(t)$ and $F_2^b(t)$, as given by Eq. 2.17.
3. Inertia forces of each rigid abutment-foundation system, with masses M_{f1} and M_{f2}, and accelerations $-\omega^2\Delta_1 e^{i\omega t}$ and $-\omega^2\Delta_2 e^{i\omega t}$, as shown in Fig. II-1-b.

The balance of the forces for the two abutment-foundation systems is then

$$\left.\begin{aligned} -\omega^2\Delta_1 M_{f1} &= -\left[-F_1^* + K_{11}\Delta_1 + K_{12}\Delta_2 + F_1^b(t)\right] \\ -\omega^2\Delta_2 M_{f2} &= -\left[-F_2^* + K_{21}\Delta_1 + K_{22}\Delta_2 + F_2^b(t)\right] \end{aligned}\right\} \quad . \tag{2.21}$$

Introducing

$$\begin{Bmatrix} M_{s1} \\ M_{s2} \end{Bmatrix} = \frac{\pi}{2}\rho_s \begin{Bmatrix} R_1^2 \\ R_2^2 \end{Bmatrix} \quad , \tag{2.22}$$

which corresponds to the mass of the soil per unit length removed by the two foundations and by using Eqs. 2.17 and 2.21 there follows:

$$\begin{bmatrix} \left[\frac{k_s R_1}{2}\left(\frac{M_{f1}}{M_{s1}} + \frac{M_b}{M_{s1}}\frac{\cot(k_b L)}{(k_b L)}\right) - \bar{K}_{11}\right] & \left[-\frac{k_s R_1}{2}\left(\frac{M_b}{M_{s1}}\frac{\operatorname{cosec}(k_b L)}{(k_b L)}\right) - \bar{K}_{12}\right] \\ \left[-\frac{k_s R_2}{2}\left(\frac{M_b}{M_{s2}}\frac{\operatorname{cosec}(k_b L)}{(k_b L)}\right) - \bar{K}_{21}\right] & \left[\frac{k_s R_2}{2}\left(\frac{M_{f2}}{M_{s2}} + \frac{M_b}{M_{s2}}\frac{\cot(k_b L)}{(k_b L)}\right) - \bar{K}_{22}\right] \end{bmatrix} \begin{Bmatrix} \Delta_1 \\ \Delta_2 \end{Bmatrix}$$

$$= \begin{Bmatrix} \bar{F}_1^* \\ \bar{F}_2^* \end{Bmatrix} \quad , \tag{2.23}$$

where

$$\begin{Bmatrix} K_{11} \\ K_{12} \end{Bmatrix} = \mu_s \pi k_s R_1 \begin{Bmatrix} \bar{K}_{11} \\ \bar{K}_{12} \end{Bmatrix} \quad , \quad \begin{Bmatrix} K_{21} \\ K_{22} \end{Bmatrix} = \mu_s \pi k_s R_2 \begin{Bmatrix} \bar{K}_{21} \\ \bar{K}_{22} \end{Bmatrix} \quad ,$$

and

$$\begin{Bmatrix} F_1^* \\ F_2^* \end{Bmatrix} = \mu_s \pi k_s \begin{Bmatrix} R_1 \bar{F}_1^* \\ R_2 \bar{F}_2^* \end{Bmatrix} \quad . \tag{2.24}$$

The foundation displacement amplitudes Δ_1 and Δ_2 are uniquely determined by solving the two simultaneous, complex, and non-homogeneous equations (Eq. 2.23).

Numerical examples presented in Figs. II-3 through II-12 depend mainly on the angle of incident waves θ and five other dimensionless parameters:

1. $\eta = \frac{\omega}{\beta_s} R_1 = k_s R_1 = \frac{2\pi}{\lambda_s} R_1$, which is the dimensionless frequency which compares the wavelength λ_s of the incident wave to the width of the left foundation.
2. $\frac{M_{f1}}{M_{s1}}$ and $\frac{M_{f2}}{M_{s2}}$, which are the ratios of the masses of the abutment-foundation systems to the masses of the soil replaced by the foundation only. They are set equal in the examples considered in this paper $\left(\text{i.e., } \frac{M_{f1}}{M_{s1}} = \frac{M_{f2}}{M_{s2}} = \frac{MF}{MS} \right)$.
3. $\frac{M_b}{M_{s1}}$ and $\frac{M_b}{M_{s2}}$, which are the ratios of the mass of the bridge girder to the masses of the soil replaced by its foundations. (In the figures these are denoted by $\frac{MB}{MS}$ when $R_1 = R_2$ and by $\frac{MB}{MS1}$ and $\frac{MB}{MS2}$ when $R_1 \neq R_2$.)

4. $\epsilon = \frac{k_b L}{k_s R_2} = \frac{\beta_s}{\beta_b} \frac{L}{R_2} = \frac{\beta_s}{\beta_b} \frac{L}{R_1} \cdot \frac{R_1}{R_2}$; this ratio reflects the relative stiffness of the bridge and the soil; it also describes the ratio of the span to the radius of the foundation. Large values of ϵ indicate a more flexible bridge with respect to the soil and/or a longer span, while $\epsilon = 0$ implies a rigid structure composed of a rigid bridge girder, rigid abutments and rigid foundations. In that case $\Delta_1 = \Delta_2$.

5. $\frac{R_1}{R_2}$; this geometric parameter which reflects the relative width of the two foundations is also needed unless $R_1 = R_2$. For different types of soil and a typical reinforced concrete structure "bridge" with μ , γ, and β as shown in Table II-1 and for selected rations of $\frac{L}{R_2}$ and $\frac{R_1}{R_2}$, the range of values for ϵ is as shown in Table II-2.

Typical Values of μ, γ and β for Reinforced

Concrete Girder Bridge and Different "Soils"

Property	Superstructure R. C. Girder Bridge	Different Soils			
		I	II	III	IV
μ K/ft^2	288,000	1,400	5,130	15,530	388,200
γ K/ft^3	0.15	0.125	0.125	0.125	0.125
β ft/sec	7,000	600	1,150	2,000	10,000
β_b/β_s		13.17	6.87	3.95	0.79

μ = shear modulus
γ = weight per unit volume
β = shear wave speed, β_b for the bridge and β_s for the soil

TABLE II-1

The Range of Values for ϵ

$\epsilon = \frac{k_b L}{k_s R_2} = \frac{\beta_s}{\beta_b} \frac{L}{R_2}$	Different Soils				L/R_2	R_1/R_2
	I	II	III	IV		
	0.39	0.73	1.27	6.33	5	1
	0.78	1.46	2.54	12.66	10	1
	1.17	2.19	3.81	18.99	15	1
	0.20	0.37	0.64	3.27	5	2
	0.39	0.73	1.27	6.33	10	2
	0.59	1.10	1.91	9.80	15	2
	0.13	0.24	0.42	2.11	5	3
	0.25	0.46	0.84	4.22	10	3
	0.38	0.73	1.26	6.33	15	3

TABLE II-2

II-5. Interpretation of the Interaction

The two displacement amplitudes Δ_1 and Δ_2 computed for the excitation corresponding to the incident plane harmonic SH-waves have been illustrated in Figs. II-3 through II-12. The displacement of the left foundation Δ_1 is represented by a dashed line, and the displacement of the right foundation Δ_2 by a solid line. These two displacement amplitudes have been plotted against the dimensionless frequency η .

Different cases have been considered which correspond to the following parameters:

1. The mass ratios have been considered in four cases:
   a. $\frac{MF}{MS} = 2$, $\frac{MB}{MS} = 2$
   b. $\frac{MF}{MS} = 4$, $\frac{MB}{MS} = 2$
   c. $\frac{MF}{MS} = 2$, $\frac{MB}{MS} = 4$
   d. $\frac{MF}{MS} = 2$, $\frac{MB}{MS2} = 2$, $\frac{MB}{MS1} = 8$
2. The following geometric size ratios were examined: $\frac{L}{R_2} = 5, 10$, for $\frac{R_1}{R_2} = 1, 2$, respectively.
3. The relative stiffness ratio of the bridge girder and the soil, which is represented by the parameter ϵ (Note: ϵ is written as EPS in these graphs), has been assumed to have the values 1, 2, 3, and 4 .
4. The angle of incidence, θ , of plane SH-waves has taken the values equal to 0° , 45°, 90°, 135° and 180° . (Note: In the case of $R_1 = R_2$, only 0°, 45°, and 90° have been shown because of symmetry.)

The figures have been arranged so that the influence of the angle of incidence and the relative stiffness ratio can be studied for the mass ratios and the geometric size ratios fixed in each figure. Each of these figures consists of parts a, b, c, and d which correspond to different values of ϵ.

Some of the most important phenomena of the interaction of the bridge and the soil through the two rigid abutment-foundation systems and the dynamic characteristics of the bridge girder response are as follows:

1. As $\epsilon \to 0$, $\Delta_1 \to \Delta_2$ (from Eq. 2.23). In that case, one has a rigid structure composed of three elements (two foundations, two abutments and a girder) all acting as a rigid body. Fig. II-3-a illustrates this case for ϵ small. When ϵ increases, the differences between Δ_1 and Δ_2 become more apparent. One notes, however, that in all cases these amplitudes approach the low frequency limit of $|\Delta_1| = |\Delta_2| = 2$, which corresponds to the displacement amplitude of the surface of the half-space for incident SH-waves with unit amplitude.
   The amplitude Δ_1 may become larger than Δ_2 due to the amplification effect caused by the scattering from the right foundation. In the cases of $\epsilon = 1.5$ in Fig. II-3-d, for example, or for $\epsilon = 2.0$ in Figs. II-4-b and II-5-b, the peaks of Δ_1 are considerably larger than 2 for small dimensionless frequencies.
2. In the case of $\theta = 90^\circ$, when $R_1 = R_2$, the two foundations are in phase and have the same amplitude. These amplitudes

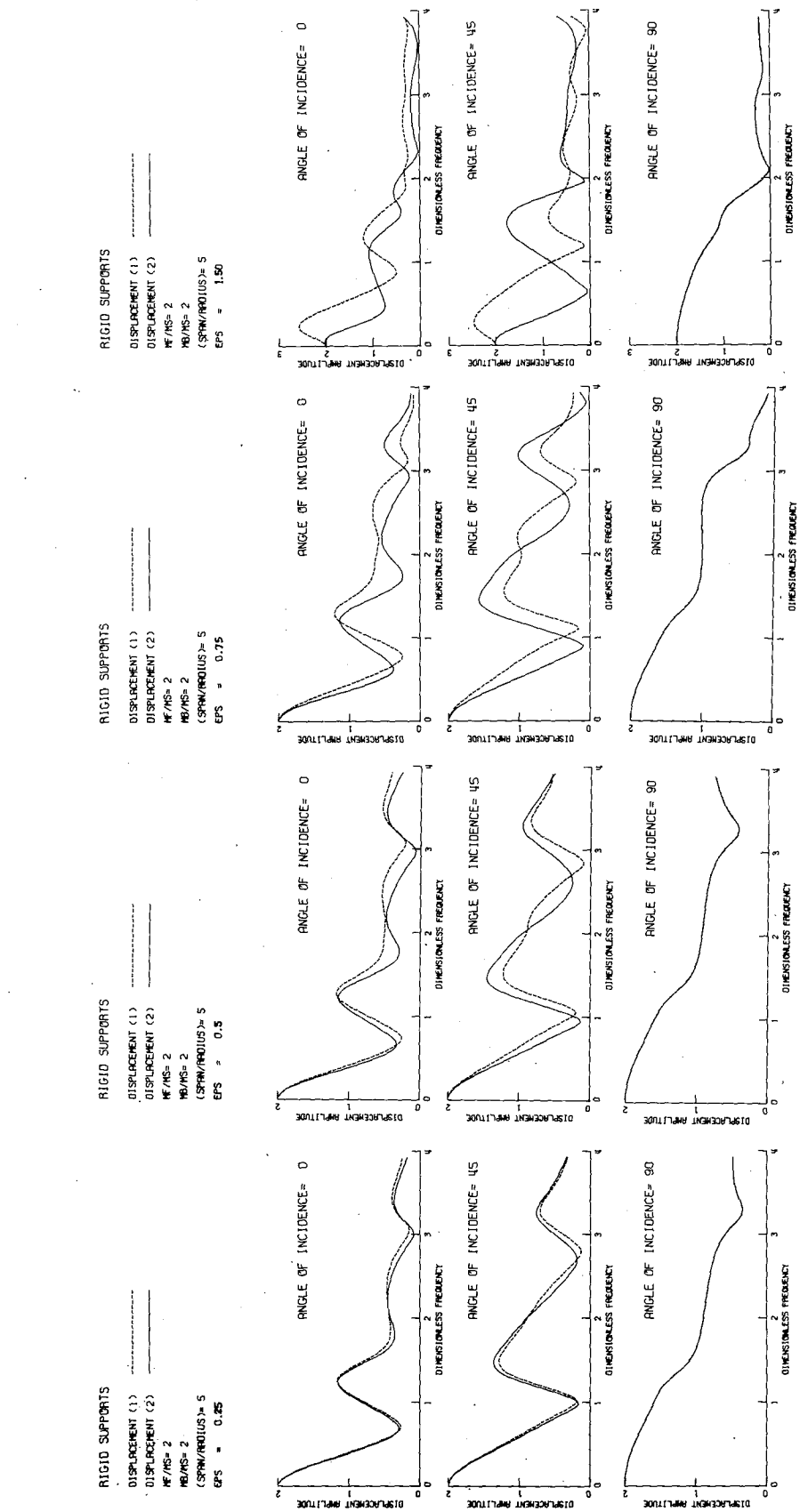
RIGID SUPPORTS
DISPLACEMENT (1) ----------
DISPLACEMENT (2) ——————
MF/MS= 2
MB/MS= 2
(SPAN/RADIUS)= 5
EPS = 0.25
RIGID SUPPORTS
DISPLACEMENT (1) ----------
DISPLACEMENT (2) ——————
MF/MS= 2
MB/MS= 2
(SPAN/RADIUS)= 5
EPS = 0.5
RIGID SUPPORTS
DISPLACEMENT (1) ----------
DISPLACEMENT (2) ——————
MF/MS= 2
MB/MS= 2
(SPAN/RADIUS)= 5
EPS = 0.75
RIGID SUPPORTS
DISPLACEMENT (1) ----------
DISPLACEMENT (2) ——————
MF/MS= 2
MB/MS= 2
(SPAN/RADIUS)= 5
EPS = 1.50
ANGLE OF INCIDENCE= 0
ANGLE OF INCIDENCE= 45
ANGLE OF INCIDENCE= 90
DISPLACEMENT AMPLITUDE
DIMENSIONLESS FREQUENCY

Fig. II-3

become zero when the beam is excited at its odd frequencies, i.e., the symmetric mode-shapes. In that case

$$\eta = n\pi/\epsilon \quad , \quad n = 1, 3, 5 \ldots \, , \tag{2.25}$$

and the symmetric modes of the bridge are

$$W_n(x) = (\sin n\pi x)/L \quad , \quad n = 1, 3, 5, \ldots \quad . \tag{2.26}$$

Thus, when $\theta = 90^\circ$ and $R_1 = R_2$, the symmetry of vibration reduces mathematically to a single foundation problem [2, 3]. When incident waves have a frequency corresponding to a fixed base frequency of this structure, the foundation(s) is(are) located at a node of the standing wave pattern and the structure above and the soil below are moving 180° out of phase.

3. The dip of the displacement amplitude curve Δ_2, which occurs for a shallow angle of incidence $\theta = 0^\circ$, 45°, is displaced towards the lower values of the dimensionless frequency η, as the flexibility of the bridge increases (Figs. II-4 and II-7). If one compares Figs. II-4 and II-6 and II-7 and II-9, one notes that, for the same ϵ and the same L/R_2, as the mass of the bridge increases, the dip moves again towards low values of η, i.e., the frequency decreases.

This behavior can be qualitatively explained by the simplified model consisting of three masses and several springs (shown in Fig. II-2-ii) where the spring constants k_1, k_2, and k_{12} depend upon the soil properties, while the spring constant k_{13} depends on the bridge stiffness. The displacements resulting from simple excitation, shown in Fig. II-2-ii, can be deter-

mined from the following matrix equation

$$\begin{bmatrix} -\omega^2 m_1 + k_1 + k_{13} + k_{12} & -k_{12} & -k_{13} \\ -k_{12} & -\omega^2 m_2 + k_2 + k_{13} + k_2 & -k_{13} \\ -k_{13} & -k_{13} & -\omega^2 m_3 + 2k_{13} \end{bmatrix} \begin{Bmatrix} X_1 \\ X_2 \\ X_3 \end{Bmatrix} = \begin{Bmatrix} k_1 \\ 0 \\ 0 \end{Bmatrix} , \tag{2.27}$$

where X_1 , X_2 and X_3 are the displacement amplitudes of the three masses. $X_2 = 0$ when $k_{12}(-\omega^2 m_3 + 2k_{13}) + k_{13}^2 = 0$, i.e.,

$$\omega_* = \sqrt{\frac{k_{13}\left(2 + \frac{k_{13}}{k_{12}}\right)}{m_3}} \quad . \tag{2.28}$$

This frequency depends on the absolute stiffness of the bridge k_{13} and the ratio of stiffness of the bridge with respect to the soil underneath it k_{13}/k_{12} . As the stiffness of the bridge k_{13} or the stiffness ratio k_{13}/k_{12} decrease, the frequency for which the dip occurs decreases (e.g., Figs. II-4, II-6, II-7 and II-9). This frequency also decreases when the mass of the bridge increases. The above model is, of course, only a simple one-dimensional analogue, while the problem under consideration is a two-dimensional one involving propagation, reflection and scattering of waves from the rigid foundations in the soil and inside the beam. Nevertheless, in spite of its one-dimensional simplicity, the above model does allow one to obtain an approximate physical understanding of a more complicated wave propagation problem.

4. In all cases which have been shown in the figures for the non-vertical incidence of waves and when $\eta = n\pi/\epsilon$, $n = 1, 2, 3, \ldots$, (i.e., when the frequency of the incident waves corresponds to the natural frequencies of the girder), one finds that $|\Delta_1| = |\Delta_2|$. As was mentioned before, $\Delta_1 = \Delta_2$ for $n = 1, 3, 5, \ldots$ and $\Delta_1 = -\Delta_2$ for $n = 2, 4, 6, \ldots$; i.e., the two end displacements are 180° out of phase. This observation gives a better idea about the phase difference between the two amplitudes Δ_1 and Δ_2, as shown, for example, in Fig. II-10. In some cases, $\Delta_1 = \Delta_2 \simeq 0$ at $\eta = n\pi/\epsilon$, $n = 1, 2, 3, 5$, as in Figs. II-5-b, II-7, II-8 and II-9-c for the second mode, Fig. II-7-c for the first mode, and Fig. II-8-c for the third mode.

5. The peak amplitudes of the displacements Δ_1 and Δ_2 may be relatively high in some cases (e.g., Figs. II-5 through II-9). For the cases studied, these amplitudes are as much as four times greater than they would be if the foundations did not interact with the soil. These peaks occur at frequencies which increase as the parameter ϵ increases for a constant span. Therefore, the more flexible the girder, the higher the frequency at which the peak occurs. Increasing the span while holding ϵ constant decreases the frequencies of these peaks. This corresponds to increasing the rigidity of the bridge with respect to that of the soil since $\epsilon = \frac{\beta_s}{\beta_b} \frac{L}{R_2}$.

6. When the mass of the foundations increases with respect to that of the girder, the peak values of the Δ_1 and Δ_2 amplitudes increase moderately. This additional increase results from increasing the span, which also decreases the significance of the interaction (e.g., Figs. II-5 and II-8).
7. When the mass of the girder increases with respect to that of the foundation (e.g., Figs. II-6 and II-9), the peak amplitudes of Δ_1 and Δ_2 decrease appreciably. As the span increases, this effect becomes less pronounced.
8. In general, as the span L increases, there is a greater degree of fluctuation in both Δ_1 and Δ_2 amplitudes. For constant L, the fluctuations of Δ_1 and Δ_2 decrease as the angle of incidence θ approaches 90°, since in that case the projected wavelength on the horizontal surface $\lambda_s^* = \lambda_s/\cos\theta$ becomes infinite.
9. When the sizes of the two foundations differ, more complicated interaction phenomena occur (Figs. II-11 and II-12):
   a. When the incident wave first hits the larger foundation (the left one), i.e., when $\theta = 0^\circ$ or 45°, this foundation acts as a shield for the right foundation. This shielding effect is most evident in Figs. II-11-a, b and II-12-a, where the smaller foundation moves with nearly the same displacement as the larger one. The additional amplification effects caused by the smaller foundation are negligible in all these cases because of the massiveness of the larger foundation.

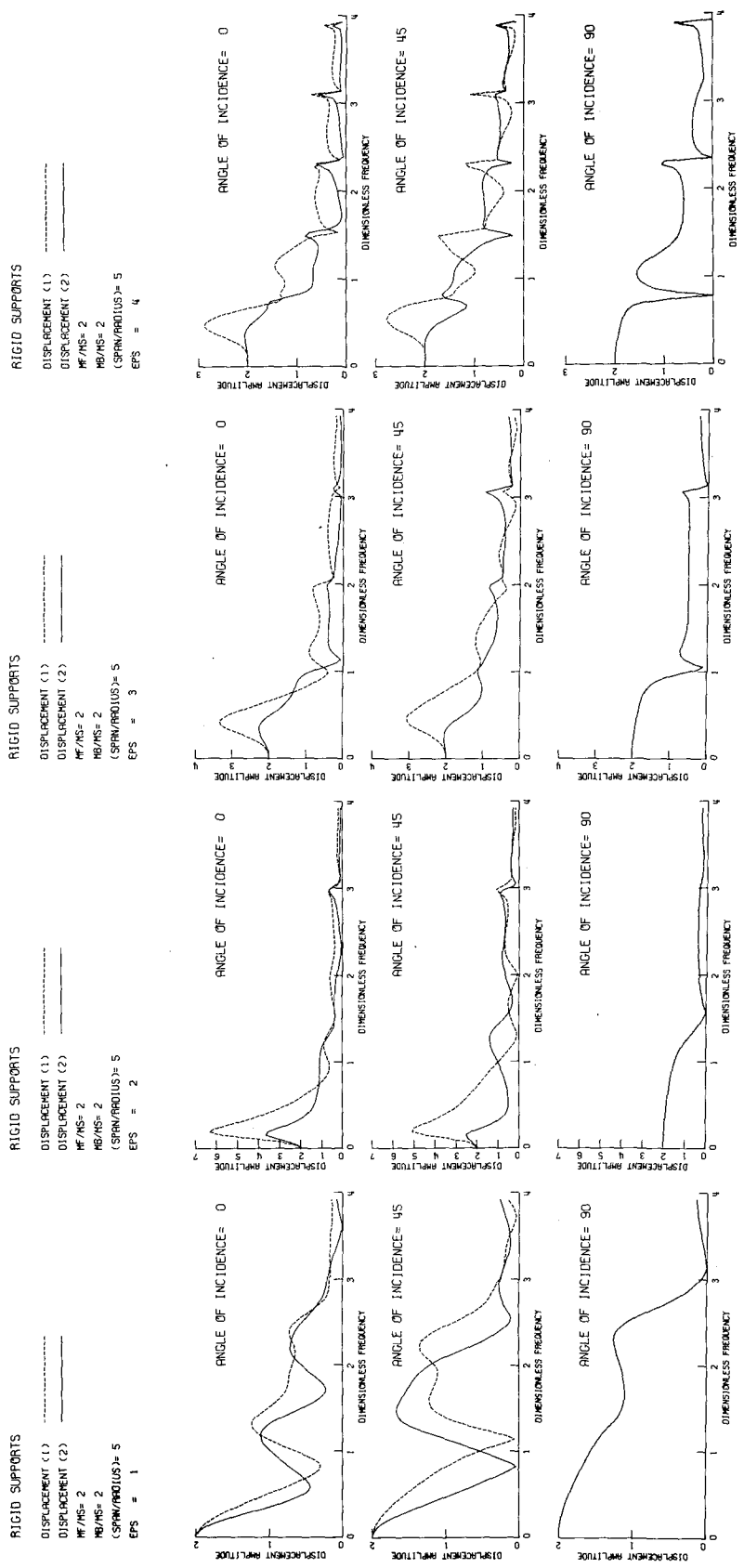
RIGID SUPPORTS
DISPLACEMENT (1) ----------
DISPLACEMENT (2) ——————
MF/MS= 2
MB/MS= 2
(SPAN/RADIUS)= 5
EPS = 1
EPS = 2
EPS = 3
EPS = 4
ANGLE OF INCIDENCE= 0
ANGLE OF INCIDENCE= 45
ANGLE OF INCIDENCE= 90
DISPLACEMENT AMPLITUDE
DIMENSIONLESS FREQUENCY

Fig. II-4

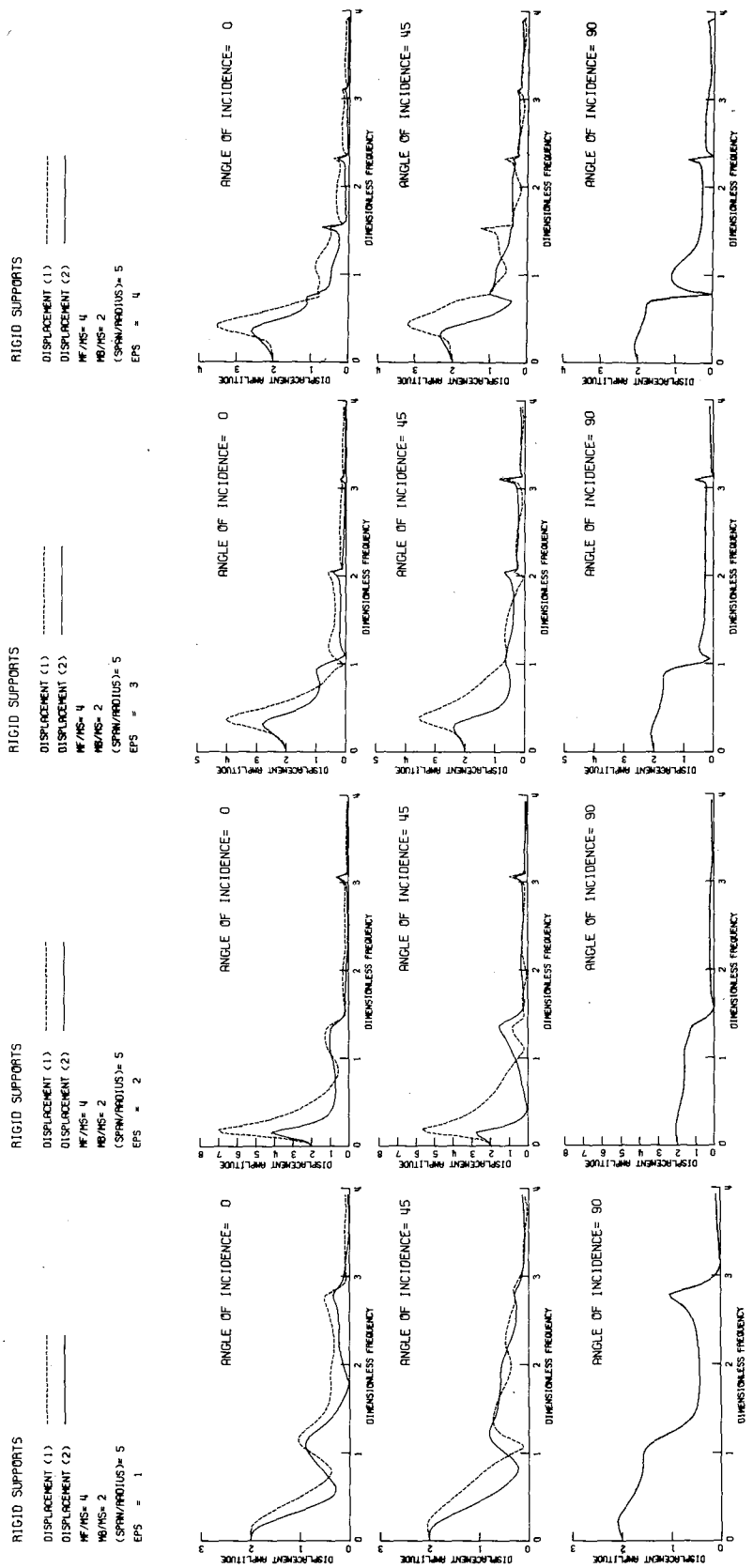
RIGID SUPPORTS
DISPLACEMENT (1) ----------
DISPLACEMENT (2) ——————
MF/MS= 4
MB/MS= 2
(SPAN/RADIUS)= 5
EPS = 1
EPS = 2
EPS = 3
EPS = 4
ANGLE OF INCIDENCE= 0
ANGLE OF INCIDENCE= 45
ANGLE OF INCIDENCE= 90
DISPLACEMENT AMPLITUDE
DIMENSIONLESS FREQUENCY

Fig. II-5

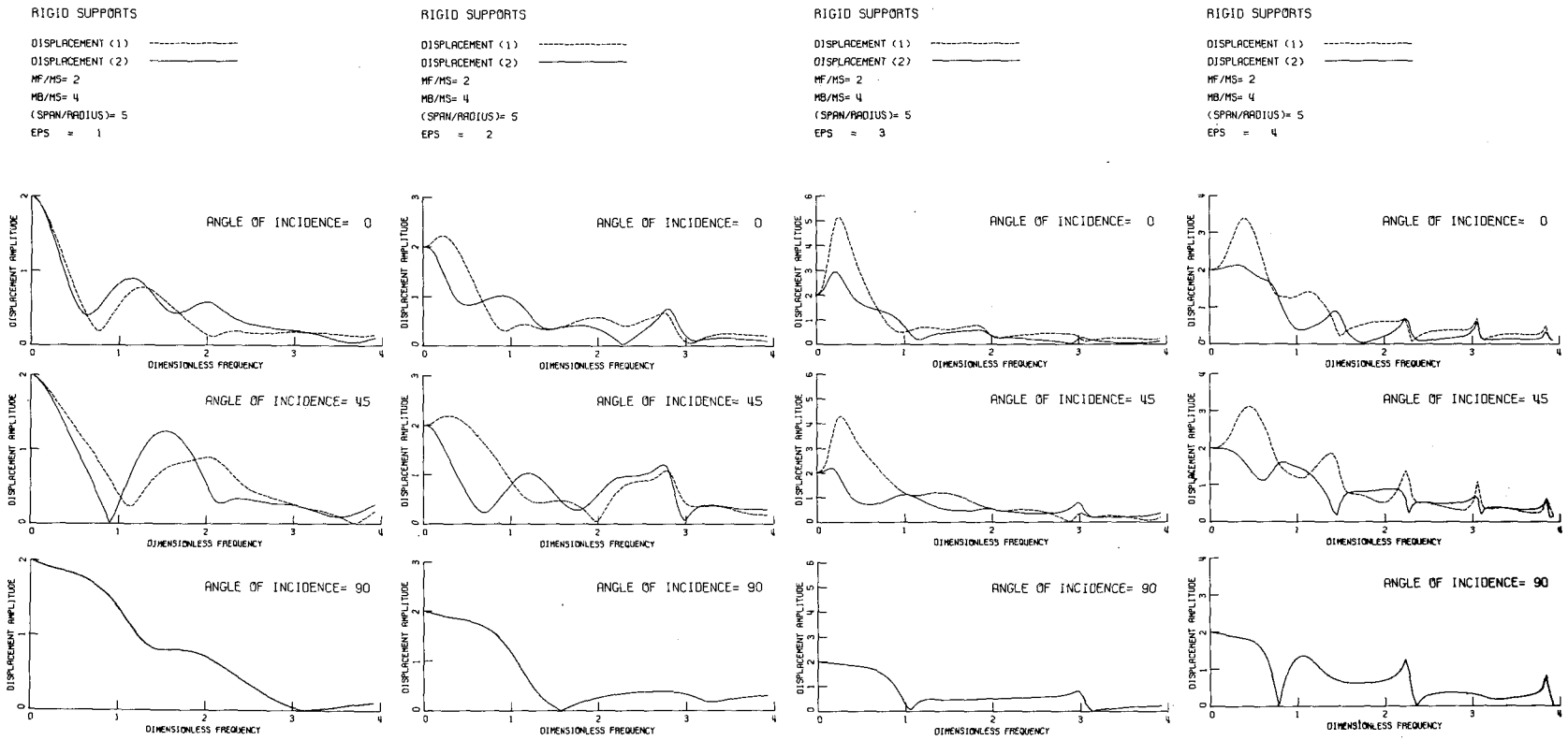
RIGID SUPPORTS
DISPLACEMENT (1)
DISPLACEMENT (2)
MF/MS= 2
MB/MS= 4
(SPAN/RADIUS)= 5
EPS = 1
RIGID SUPPORTS
DISPLACEMENT (1)
DISPLACEMENT (2)
MF/MS= 2
MB/MS= 4
(SPAN/RADIUS)= 5
EPS = 2
RIGID SUPPORTS
DISPLACEMENT (1)
DISPLACEMENT (2)
MF/MS= 2
MB/MS= 4
(SPAN/RADIUS)= 5
EPS = 3
RIGID SUPPORTS
DISPLACEMENT (1)
DISPLACEMENT (2)
MF/MS= 2
MB/MS= 4
(SPAN/RADIUS)= 5
EPS = 4
ANGLE OF INCIDENCE= 0
ANGLE OF INCIDENCE= 45
ANGLE OF INCIDENCE= 90
DISPLACEMENT AMPLITUDE
DIMENSIONLESS FREQUENCY

Fig. II-6

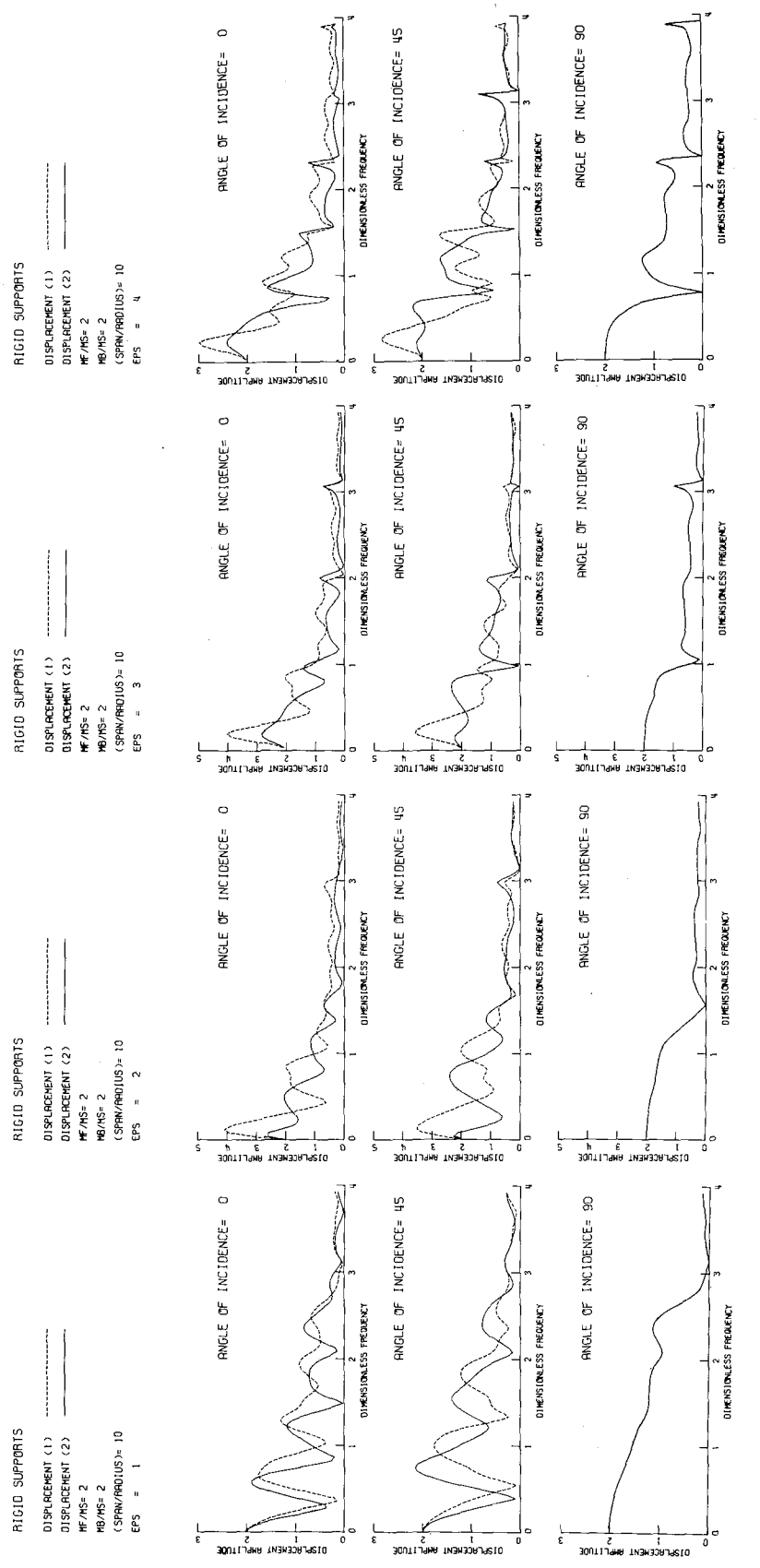
RIGID SUPPORTS
DISPLACEMENT (1) ----------
DISPLACEMENT (2) ——————
MF/MS= 2
MB/MS= 2
(SPAN/RADIUS)= 10
EPS = 1
RIGID SUPPORTS
DISPLACEMENT (1) ----------
DISPLACEMENT (2) ——————
MF/MS= 2
MB/MS= 2
(SPAN/RADIUS)= 10
EPS = 2
RIGID SUPPORTS
DISPLACEMENT (1) ----------
DISPLACEMENT (2) ——————
MF/MS= 2
MB/MS= 2
(SPAN/RADIUS)= 10
EPS = 3
RIGID SUPPORTS
DISPLACEMENT (1) ----------
DISPLACEMENT (2) ——————
MF/MS= 2
MB/MS= 2
(SPAN/RADIUS)= 10
EPS = 4
ANGLE OF INCIDENCE= 0
ANGLE OF INCIDENCE= 45
ANGLE OF INCIDENCE= 90
DISPLACEMENT AMPLITUDE
DIMENSIONLESS FREQUENCY

Fig. II-7

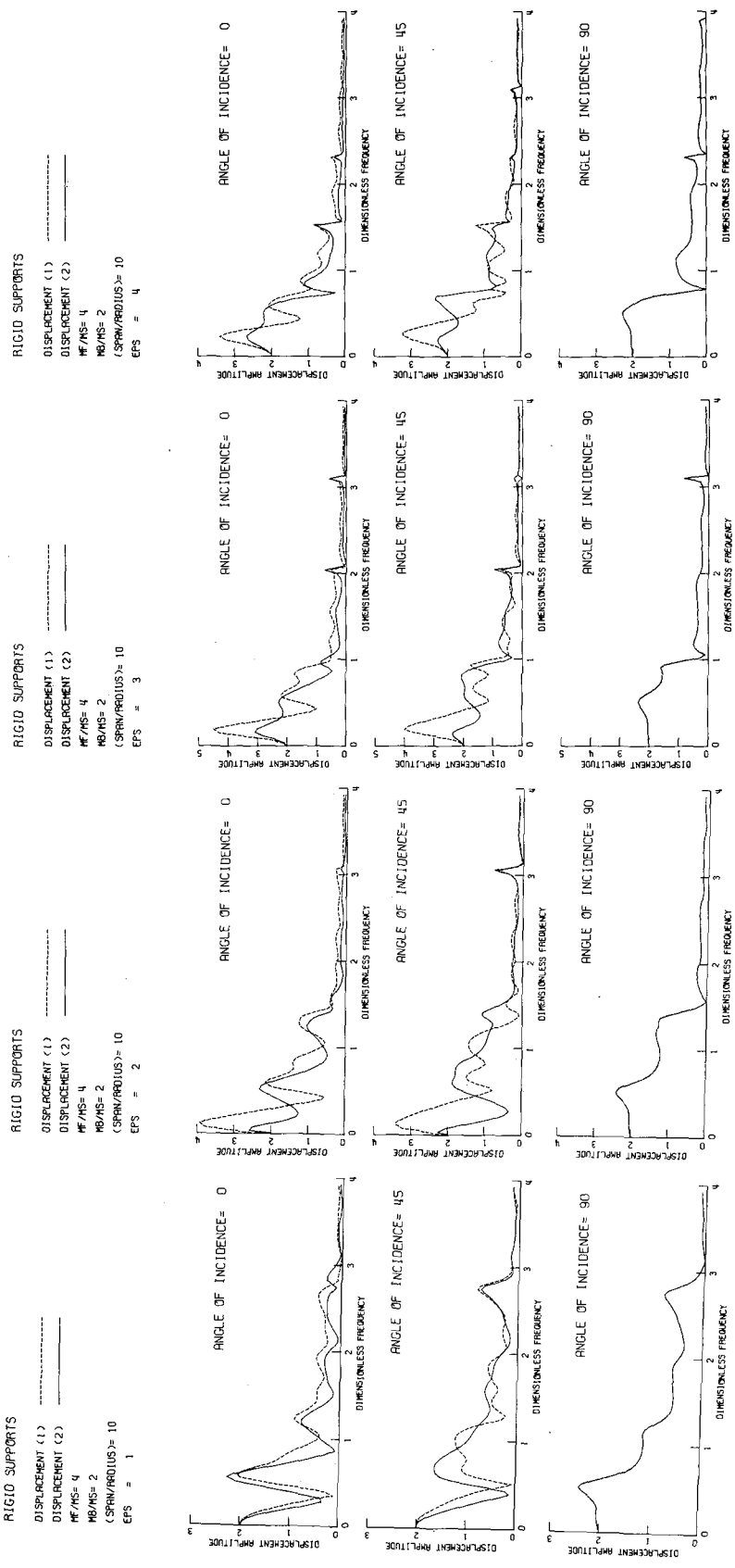
RIGID SUPPORTS
DISPLACEMENT (1) ----------
DISPLACEMENT (2) ——————
MF/MS= 4
MB/MS= 2
(SPAN/RADIUS)= 10
EPS = 1
RIGID SUPPORTS
DISPLACEMENT (1) ----------
DISPLACEMENT (2) ——————
MF/MS= 4
MB/MS= 2
(SPAN/RADIUS)= 10
EPS = 2
RIGID SUPPORTS
DISPLACEMENT (1) ----------
DISPLACEMENT (2) ——————
MF/MS= 4
MB/MS= 2
(SPAN/RADIUS)= 10
EPS = 3
RIGID SUPPORTS
DISPLACEMENT (1) ----------
DISPLACEMENT (2) ——————
MF/MS= 4
MB/MS= 2
(SPAN/RADIUS)= 10
EPS = 4
ANGLE OF INCIDENCE= 0
ANGLE OF INCIDENCE= 45
ANGLE OF INCIDENCE= 90
DISPLACEMENT AMPLITUDE
DIMENSIONLESS FREQUENCY

Fig. II-8

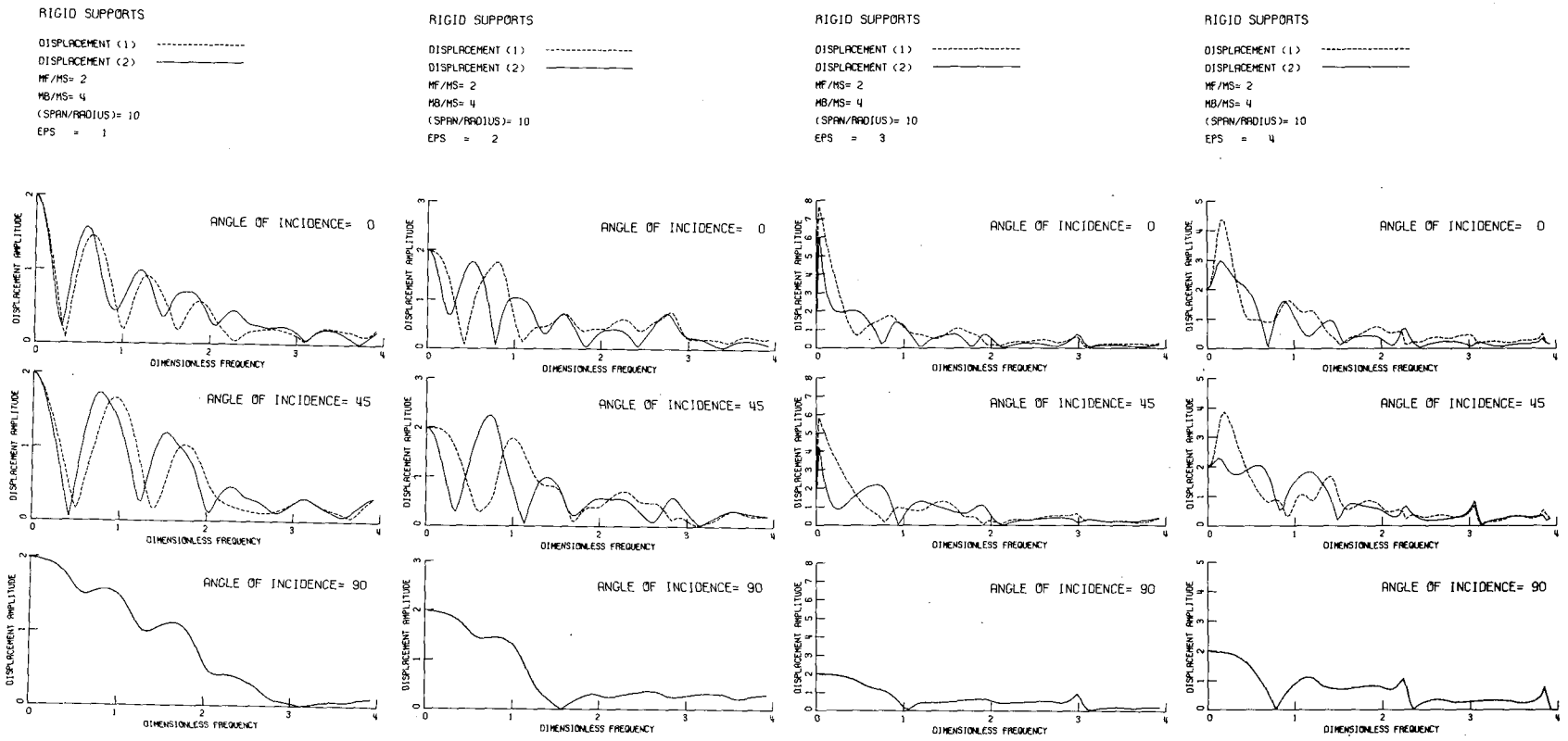
RIGID SUPPORTS
DISPLACEMENT (1)
DISPLACEMENT (2)
MF/MS= 2
MB/MS= 4
(SPAN/RADIUS)= 10
EPS = 1
RIGID SUPPORTS
DISPLACEMENT (1)
DISPLACEMENT (2)
MF/MS= 2
MB/MS= 4
(SPAN/RADIUS)= 10
EPS = 2
RIGID SUPPORTS
DISPLACEMENT (1)
DISPLACEMENT (2)
MF/MS= 2
MB/MS= 4
(SPAN/RADIUS)= 10
EPS = 3
RIGID SUPPORTS
DISPLACEMENT (1)
DISPLACEMENT (2)
MF/MS= 2
MB/MS= 4
(SPAN/RADIUS)= 10
EPS = 4
ANGLE OF INCIDENCE= 0
ANGLE OF INCIDENCE= 45
ANGLE OF INCIDENCE= 90
DISPLACEMENT AMPLITUDE
DIMENSIONLESS FREQUENCY

Fig. II-9

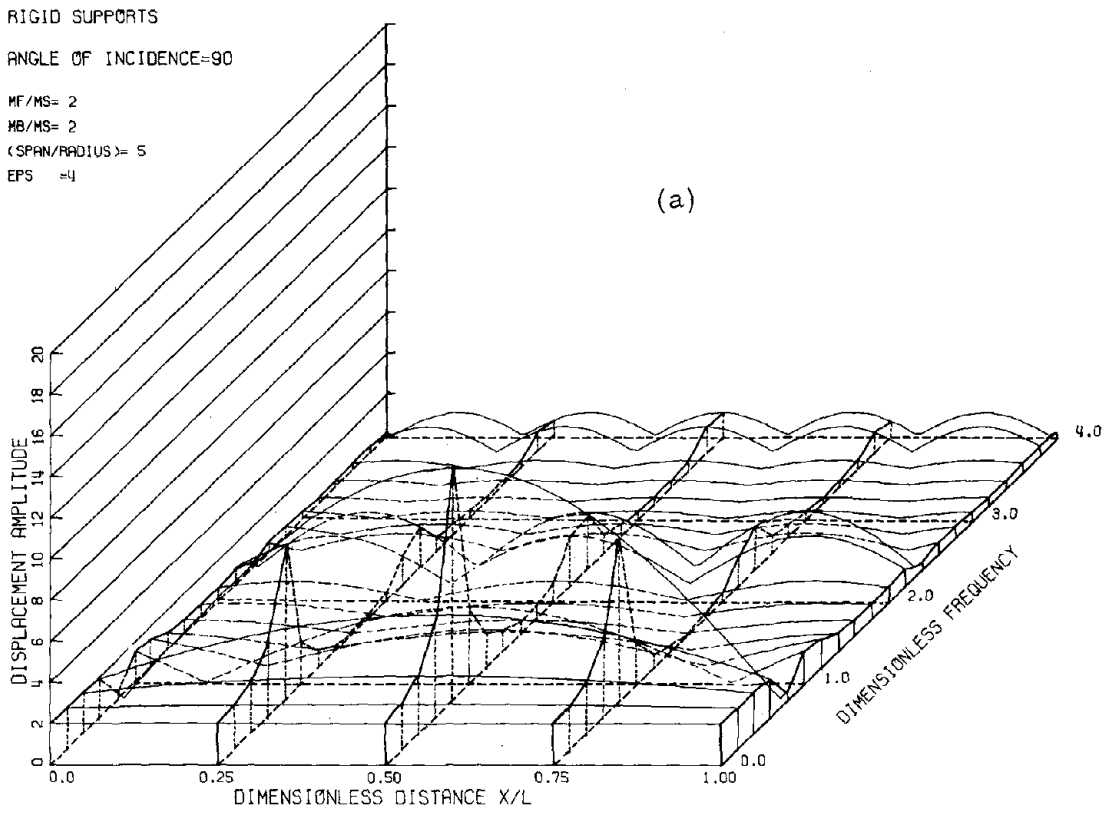
RIGID SUPPORTS
ANGLE OF INCIDENCE=90
MF/MS= 2
MB/MS= 2
(SPAN/RADIUS)= 5
EPS =4
(a)
DISPLACEMENT AMPLITUDE
0
2
4
6
8
10
12
14
16
18
20
0.0
0.25
0.50
0.75
1.00
DIMENSIONLESS DISTANCE X/L
0.0
1.0
2.0
3.0
4.0
DIMENSIONLESS FREQUENCY

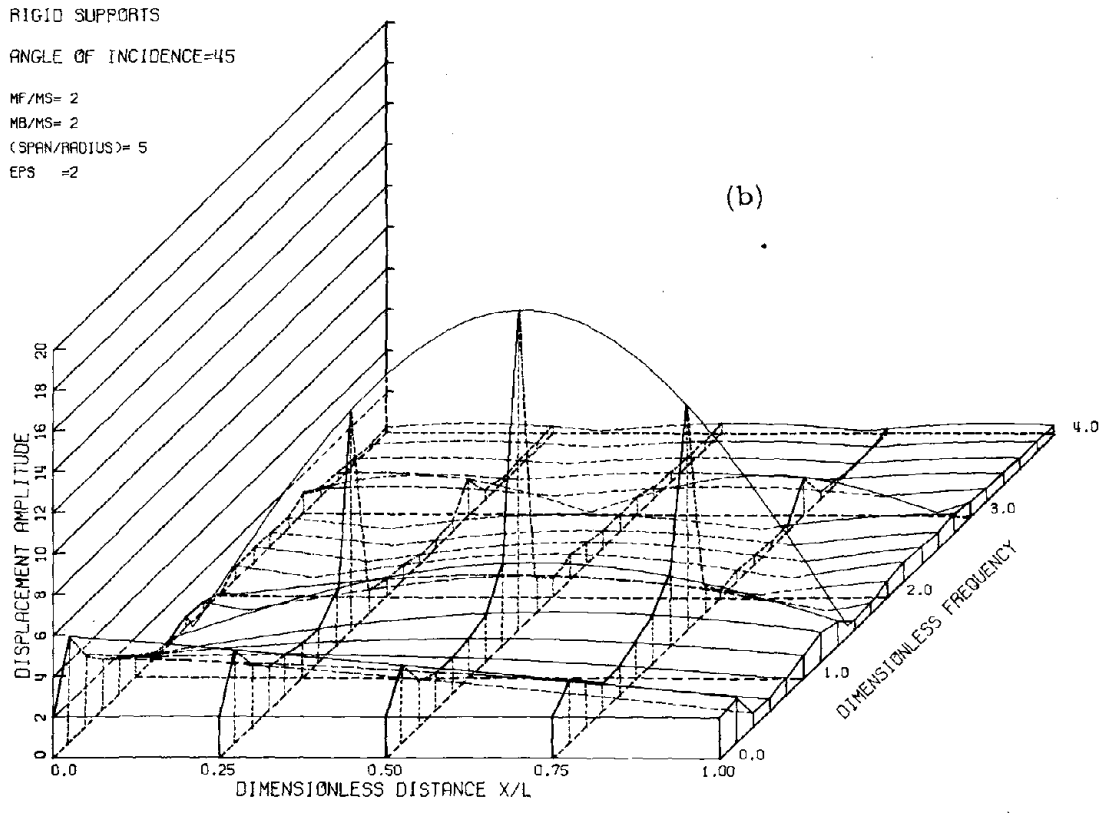
RIGID SUPPORTS
ANGLE OF INCIDENCE=45
MF/MS= 2
MB/MS= 2
(SPAN/RADIUS)= 5
EPS =2
(b)
DISPLACEMENT AMPLITUDE
0
2
4
6
8
10
12
14
16
18
20
0.0
0.25
0.50
0.75
1.00
DIMENSIONLESS DISTANCE X/L
0.0
1.0
2.0
3.0
4.0
DIMENSIONLESS FREQUENCY

Fig. II-10

The shielding effect decreases with an increase of the following parameters:

(1) the flexibility of the girder

(2) the span (Fig. II-11)

(3) the angle of incidence θ

(4) the ratio R_2/R_1 for the same span (Figs. II-11 and II-12).

b. When the incident wave first hits the smaller foundation (the right one), i.e., when $\theta = 135^\circ$ or 180°, the left foundation acts as a barrier which reflects significant wave energy back towards the small foundation while the shielding effect provided by the right foundation is negligible (Figs. II-11-b and II-12-b). The overall amplitudes of Δ_1 and Δ_2 are influenced by:

(1) the flexibility of the girder;

(2) the span and the size of the foundations; and

(3) the angle of incidence θ.

c. The peak value of the displacement amplitudes Δ_1 and Δ_2 increases with the increase of flexibility of the superstructure and the increase of ratio R_1/R_2 (Figs. II-11-b and II-12-a, b, c).

d. For both vertical and nonvertical incident waves, small amplitudes of $|\Delta_1|$ and $|\Delta_2|$ occur at $\eta = n\pi/\epsilon$, $R_1/R_2 \neq 1$, $n = 1, 3, 5, \ldots$ as shown in Figs. II-11 and II-12. Since $R_1 \neq R_2$, the bridge system is not symmetric

now and, in general, one does not expect to find that

$$|\Delta_1| = |\Delta_2| \quad \text{for all } \theta \text{ and } \eta = \frac{n\pi}{\epsilon} \frac{R_1}{R_2} .$$

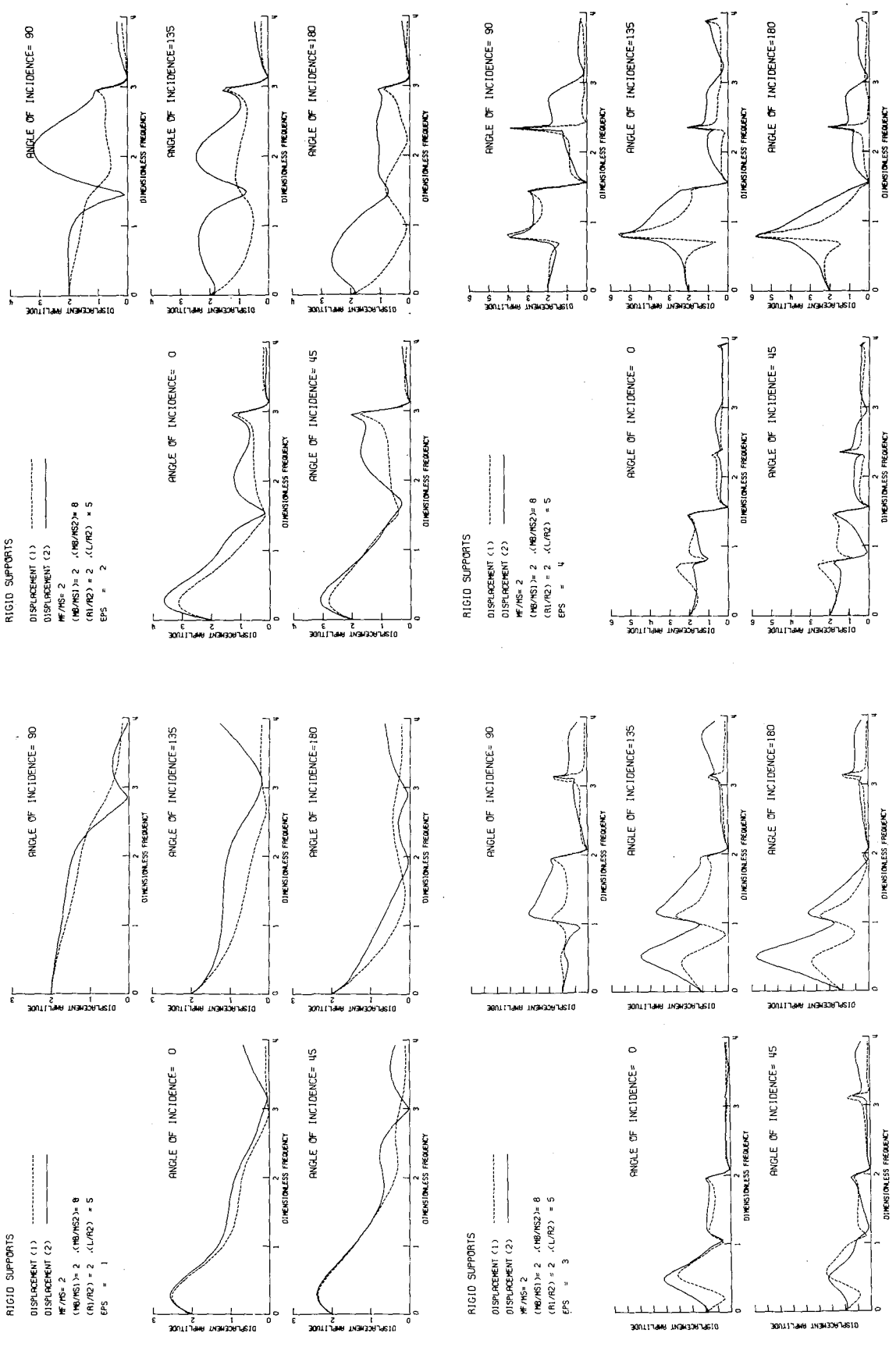
RIGID SUPPORTS
DISPLACEMENT (1) ----------
DISPLACEMENT (2) ——————
MF/MS= 2
(MB/MS)= 2 ,(MB/MS2)= 8
(R1/R2) = 2 ,(L/R2) = 5
EPS = 1
ANGLE OF INCIDENCE= 90
ANGLE OF INCIDENCE= 0
ANGLE OF INCIDENCE=135
ANGLE OF INCIDENCE= 45
ANGLE OF INCIDENCE=180
DISPLACEMENT AMPLITUDE
DIMENSIONLESS FREQUENCY
RIGID SUPPORTS
DISPLACEMENT (1) ----------
DISPLACEMENT (2) ——————
MF/MS= 2
(MB/MS)= 2 ,(MB/MS2)= 8
(R1/R2) = 2 ,(L/R2) = 5
EPS = 2
ANGLE OF INCIDENCE= 90
ANGLE OF INCIDENCE= 0
ANGLE OF INCIDENCE=135
ANGLE OF INCIDENCE= 45
ANGLE OF INCIDENCE=180
DISPLACEMENT AMPLITUDE
DIMENSIONLESS FREQUENCY
RIGID SUPPORTS
DISPLACEMENT (1) ----------
DISPLACEMENT (2) ——————
MF/MS= 2
(MB/MS)= 2 ,(MB/MS2)= 8
(R1/R2) = 2 ,(L/R2) = 5
EPS = 3
ANGLE OF INCIDENCE= 90
ANGLE OF INCIDENCE= 0
ANGLE OF INCIDENCE=135
ANGLE OF INCIDENCE= 45
ANGLE OF INCIDENCE=180
DISPLACEMENT AMPLITUDE
DIMENSIONLESS FREQUENCY
RIGID SUPPORTS
DISPLACEMENT (1) ----------
DISPLACEMENT (2) ——————
MF/MS= 2
(MB/MS)= 2 ,(MB/MS2)= 8
(R1/R2) = 2 ,(L/R2) = 5
EPS = 4
ANGLE OF INCIDENCE= 90
ANGLE OF INCIDENCE= 0
ANGLE OF INCIDENCE=135
ANGLE OF INCIDENCE= 45
ANGLE OF INCIDENCE=180
DISPLACEMENT AMPLITUDE
DIMENSIONLESS FREQUENCY

Fig. II-11

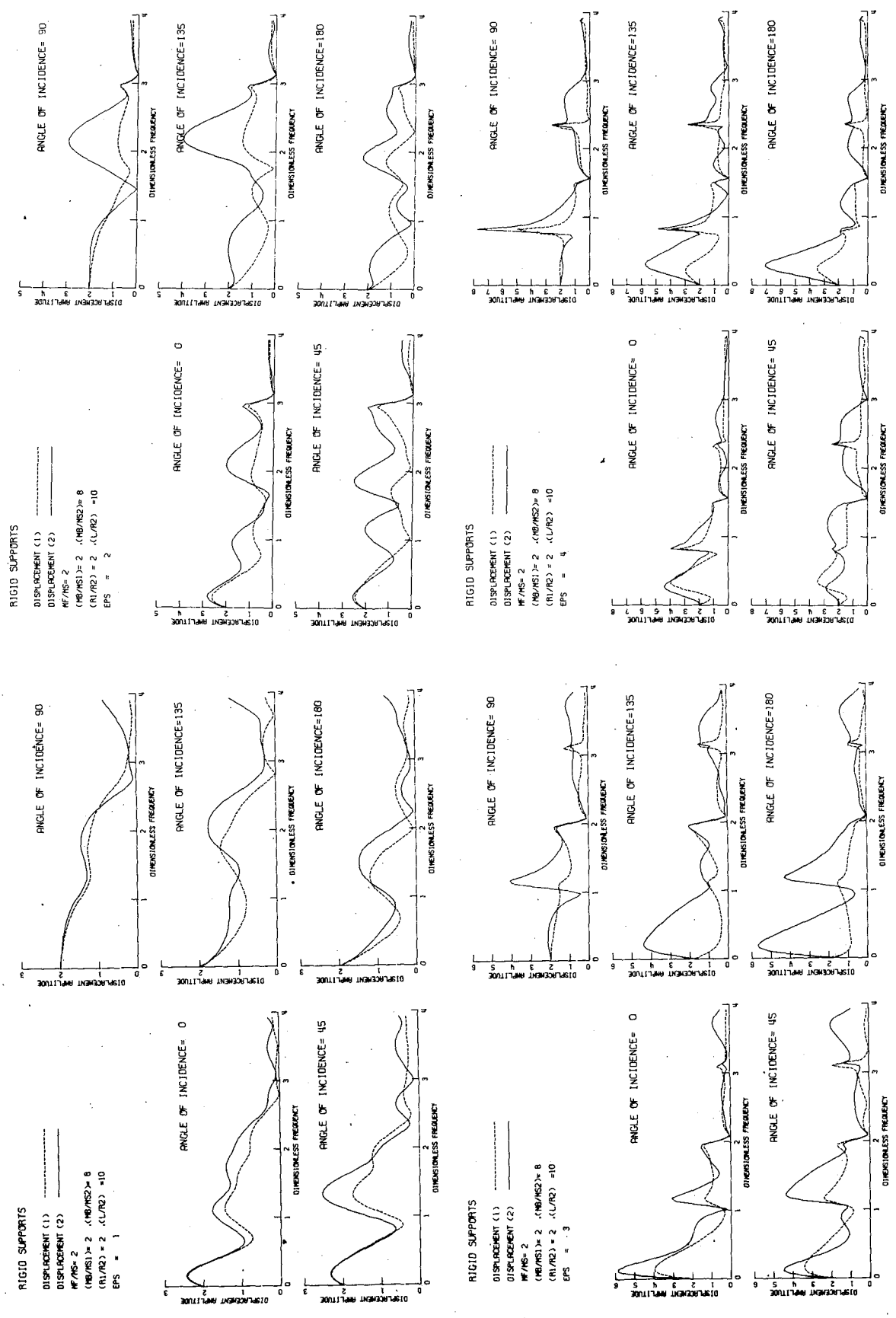
RIGID SUPPORTS
DISPLACEMENT (1) ----------
DISPLACEMENT (2) ——————
MF/MS= 2
(MB/MS1)= 2 ,(MB/MS2)= 8
(R1/R2) = 2 ,(L/R2) =10
EPS = 1
ANGLE OF INCIDENCE= 0
ANGLE OF INCIDENCE= 45
ANGLE OF INCIDENCE= 90
ANGLE OF INCIDENCE=135
ANGLE OF INCIDENCE=180
DISPLACEMENT AMPLITUDE
DIMENSIONLESS FREQUENCY
RIGID SUPPORTS
DISPLACEMENT (1) ----------
DISPLACEMENT (2) ——————
MF/MS= 2
(MB/MS1)= 2 ,(MB/MS2)= 8
(R1/R2) = 2 ,(L/R2) =10
EPS = 3
ANGLE OF INCIDENCE= 0
ANGLE OF INCIDENCE= 45
ANGLE OF INCIDENCE= 90
ANGLE OF INCIDENCE=135
ANGLE OF INCIDENCE=180
DISPLACEMENT AMPLITUDE
DIMENSIONLESS FREQUENCY
RIGID SUPPORTS
DISPLACEMENT (1) ----------
DISPLACEMENT (2) ——————
MF/MS= 2
(MB/MS1)= 2 ,(MB/MS2)= 8
(R1/R2) = 2 ,(L/R2) =10
EPS = 2
ANGLE OF INCIDENCE= 0
ANGLE OF INCIDENCE= 45
ANGLE OF INCIDENCE= 90
ANGLE OF INCIDENCE=135
ANGLE OF INCIDENCE=180
DISPLACEMENT AMPLITUDE
DIMENSIONLESS FREQUENCY
RIGID SUPPORTS
DISPLACEMENT (1) ----------
DISPLACEMENT (2) ——————
MF/MS= 2
(MB/MS1)= 2 ,(MB/MS2)= 8
(R1/R2) = 2 ,(L/R2) =10
EPS = 4
ANGLE OF INCIDENCE= 0
ANGLE OF INCIDENCE= 45
ANGLE OF INCIDENCE= 90
ANGLE OF INCIDENCE=135
ANGLE OF INCIDENCE=180
DISPLACEMENT AMPLITUDE
DIMENSIONLESS FREQUENCY

Fig. II-12

II-6. Response of the Bridge

From the Earthquake Engineering and Structural Dynamics point of view, one of the more important problems is to find which are the critical sections of a structure and to estimate where the maximum displacements or the maximum stresses may occur. With this in mind, and to illustrate the effects of soil-bridge interaction on the girder of the single-span bridge studied in this analysis, the response of the midpoint and the two quarter points ($x/L = 0.25, 0.75$), have been examined in some detail as shown in the three-dimensional Fig. II-10.

Using Eq. 2.14 for $x = L/2$, the displacement amplitude $|w(L/2, t)|$ is calculated at the midpoint of the span as:

$$w\left(\frac{L}{2}, t\right) = \left[\cos\left(\frac{k_b L}{2}\right) - \cot(k_b L)\sin\left(\frac{k_b L}{2}\right)\right]\Delta_1 + \left[\operatorname{cosec}(k_b L)\sin\left(\frac{k_b L}{2}\right)\right]\Delta_2 ,$$

which reduces to

$$\left|w\left(\frac{L}{2}, t\right)\right| = \left|\frac{(\Delta_1 + \Delta_2)}{2}\sec\left(\frac{k_b L}{2}\right)\right| . \qquad (2.29)$$

When interaction is neglected, both Δ_1 and Δ_2 would become 1, and $|w(L/2, t)|$ would become infinite at the natural frequencies of the shear beam, i.e., at $k_b L = n\pi$, $n = 1, 3, 5, \ldots$ (since there is contribution only from the symmetric modes for the midpoint). However, if interaction is not neglected by using the results from the above analysis the following can be said about the beam response:

1. When $\Delta_1 = \Delta_2 = 0$ at $\eta = n\pi/\epsilon$; $n = 1, 3, 5, \ldots$; $R_1 = R_2$; i.e., in the case of vertical SH-waves where $\theta = 90^\circ$, the response given by Eq. 2.29 remains finite and is characterized by relatively small peaks, as shown for example, in Fig. II-13. It can also be seen in this figure that when $\theta \neq 90^\circ$ the peaks, in general, are much larger and the effect of small Δ_1 and Δ_2 is less pronounced.
2. When Δ_1 and Δ_2 have considerable amplitudes at $\eta = n\pi/\epsilon$, $n = 1, 3, 5, \ldots$, and in the case of non-vertically incident SH-waves, the amplitude of the beam response is large at $\eta = n\pi/\epsilon$, i.e., at the fundamental resonant frequencies of the beam. It should be noted that the sharp peaks in Fig. II-13 have been plotted only up to the amplitude equal to 40 to preserve the detail and resolution of the neighboring smaller amplitudes.

Other important characteristics of the results which can be shown in figures similar to Fig. II-13 can be summarized as follows: In general, the peak values of $|w(L/2, t)|$ increase with ϵ, when $\theta = 90^\circ$, i.e., for higher flexibility of the structure with respect to that of the soil and for the MB/MS fixed. The peak response amplitudes decrease for the higher modes and for the same ϵ. Increasing the foundation mass [larger (MF/MS)] leads to more effective coupling of the bridge to the soil and thus less radiative damping, while increasing the mass of the girder [larger (MB/MS)] leads to higher radiative damping when L is constant. The increase of span L for a fixed value of $\left(\frac{\beta_d}{\beta_s} = \frac{L}{\epsilon R_2}\right)$, which is equivalent to

increasing the rigidity of the girder with respect to that of the soil, also leads to more radiative damping.

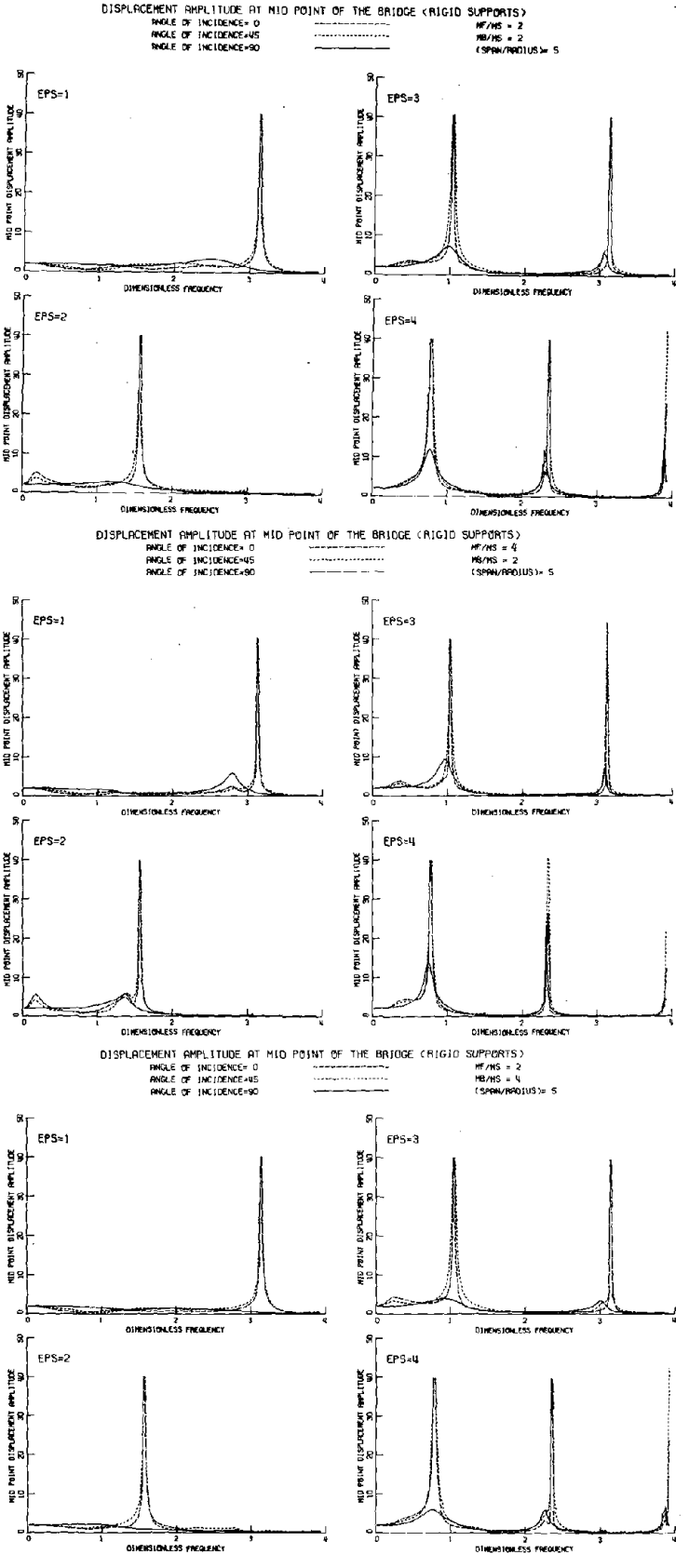
DISPLACEMENT AMPLITUDE AT MID POINT OF THE BRIDGE (RIGID SUPPORTS)
ANGLE OF INCIDENCE= 0
ANGLE OF INCIDENCE=45
ANGLE OF INCIDENCE=90
MF/MS = 2
MB/MS = 2
(SPAN/RADIUS)= 5
EPS=1
EPS=3
EPS=2
EPS=4
MID POINT DISPLACEMENT AMPLITUDE
DIMENSIONLESS FREQUENCY
DISPLACEMENT AMPLITUDE AT MID POINT OF THE BRIDGE (RIGID SUPPORTS)
ANGLE OF INCIDENCE= 0
ANGLE OF INCIDENCE=45
ANGLE OF INCIDENCE=90
MF/MS = 4
MB/MS = 2
(SPAN/RADIUS)= 5
EPS=1
EPS=3
EPS=2
EPS=4
MID POINT DISPLACEMENT AMPLITUDE
DIMENSIONLESS FREQUENCY
DISPLACEMENT AMPLITUDE AT MID POINT OF THE BRIDGE (RIGID SUPPORTS)
ANGLE OF INCIDENCE= 0
ANGLE OF INCIDENCE=45
ANGLE OF INCIDENCE=90
MF/MS = 2
MB/MS = 4
(SPAN/RADIUS)= 5
EPS=1
EPS=3
EPS=2
EPS=4
MID POINT DISPLACEMENT AMPLITUDE
DIMENSIONLESS FREQUENCY

Fig. II-13

II-7. Conclusions

A key step in the evaluation of the soil-structure interaction effects on the earthquake response of a structure is in the computation of the force-displacement relationships for the foundation. Several such relationships [2, 5, 8, 9], expressed in terms of impedance or compliance functions, are available in the literature.

Having obtained the impedance function for particular two-dimensional abutment conditions, represented by rigid foundations with semicircular cross sections, and having defined the input motion in terms of plane SH-waves, the calculation of the response of bridge girder depends on the stiffness, mass and damping characteristics of the bridge relative to that of the soil. For some input frequencies the amplitude of the foundation response has been found to be significantly larger than the free field surface displacement amplitude which could be obtained for the same excitation in the absence of a bridge or its abutments.

The excitation of different modes of vibration of the two-dimensional bridge girder is related to the nature of the foundation movement for different angles of incident SH-waves and, in particular, depends on the relative phase of motion for two bridge abutments. When two abutments move in phase, there is a tendency to excite symmetric modes of girder vibration; while when they are moving out of phase, the antisymmetric modes are excited more effectively. The simplest type of two-dimensional soil-bridge interaction occurs for the vertical incidence of SH-waves and for the symmetric bridge and its abutments. In that case, for the frequencies that

correspond to the symmetric modes of girder vibration, the two abutments do not move and the efficiency of radiation damping, which results from the wave scattering from the two foundations, is maximum. In all other cases, when the angle of incident waves is not vertical, or when the bridge girder is not symmetric and/or when the abutments are different, this simplicity is lost and the efficiency of radiative damping is significantly reduced. In general, when the angle of incident SH-waves is not vertical, large response of the bridge is obtained at the fixed base natural frequencies of the bridge.

When the bridge and its abutments are symmetric, the torsional motion of the whole bridge does not seem to be excited appreciably, at least not for the mass ratios and the geometries studied in this analysis. However, this tendency is completely reversed when the bridge abutments are not the same (i.e., $R_1 \neq R_2$ and/or MS1 $\neq$ MS2). Nonsymmetry of mass distributions enhances the overall torsional response, especially for horizontally incident SH-waves. Other related phenomena, such as shielding, amplification by the wave scattered from the other foundation, and the influence of the standing wave pattern on the excitation of two bridge abutments, are all accentuated and made more complex by the nonsymmetry of the two abutments.

REFERENCES OF CHAPTER II

1. Housner, G. W., "Interaction of Building and Ground During an Earthquake," Bulletin of the Seismological Society of America, 47, no. 3, 1957, pp. 179-186.

2. Luco, J. E., "Dynamic Interaction of a Shear Wall with the Soil," J. Eng. Mech. Div., ASCE, EM2, 1969, pp. 333-345.

3. Trifunac, M. D., "Interaction of a Shear Wall with the Soil for Incident Plane SH-Waves," Bulletin of the Seismological Society of America, 62, no. 1, 1972, pp. 63-83.

4. Seed, H. B. and Idriss, I. M., "Soil-Structure Interaction of Massive Embedded Structures During Earthquakes," 5WCEE, Rome, Italy, 1973.

5. Luco, J. E. and Contesse, L. A., "Dynamic Structure-Soil-Structure Interaction," Bulletin of the Seismological Society of America, 63, no. 4, August 1973, pp. 1284-1303.

6. Okamoto, S., Introduction to Earthquake Engineering, John Wiley and Sons, New York-Toronto, 1973, Chapter 12, pp. 301-374.

7. Wiegel, R. L., Earthquake Engineering, Prentice-Hall, Inc. Englewood Cliffs, New Jersey, 1970.

8. Luco, J. E., Wong, H. L. and Trifunac, M. D., "A Note on the Dynamic Response of Rigid Embedded Foundations," Earthquake Engineering and Structural Dynamics, 1975.

9. Wong, H. L. and Trifunac, M. D., "Two-dimensional, Antiplane, Building-Soil-Building Interaction for Two or More Buildings and for Incident Plane SH-Waves," Bulletin of the Seismological Society of America, 65, 1975.

10. Thau, S. A., "Radiation and Scattering from a Rigid Inclusion in an Elastic Medium," Journal of Applied Mechanics, 34, 1967, pp. 509-511.